1-1-2001

Sub-micron machining of materials using nonlinear liquid lenses and ultrafast lasers

Diwakar Ramanathan
Iowa State University

Sub-micron machining of materials using nonlinear liquid lenses and ultrafast lasers

by

Diwakar Ramanathan

A thesis submitted to the graduate faculty

In partial fulfillment of the requirements for the degree of

MASTER OF SCIENCE

Major: Mechanical Engineering

Program of Study Committee:
Palaniappa A. Molian (Major Professor)
Daniel Bullen
Ranga Narayanaswami

Iowa State University

Ames, Iowa

2001

Graduate College

Iowa State University

This is to certify that the master's thesis of

Diwakar Ramanathan

has met the thesis requirements of Iowa State University

Signatures have been redacted for privacy

to my family

TABLE OF CONTENTS

LIST OF FIGURES

LIST OF TABLES

ACKNOWLEDGEMENTS

I would like to express my thanks to my major professor Dr. Molian for his unstinting support during the duration of my Masters program. He helped me envision my program goals and helped me realize them successfully. The brain storming sessions with him to complete my publications were a big help in getting a better understanding of various concepts. I would also like to thank Dr. Ranga and Dr. Bullen for accepting to serve on my committee and providing inputs for the successful completion of my thesis.

My special thoughts of gratitude go to my parents for supporting my study abroad. Their hopes and aspirations helped me set my goals higher than I would have ever done. I would also like to thank the various technicians and researchers who helped me with my research at various points. Special thanks to Dr. Straszheim for his assistance in helping me with my SEM work and Jim Dautremont for his assistance in troubleshooting problems with the various equipment in the research laboratory.

CHAPTER 1. INTRODUCTION

The purpose of this work is to investigate and analyze the effects of ultrashort ($<10^{12}$ seconds) pulses in conjunction with nonlinear liquid lenses on diamond and biomedical materials. The capabilities of lasers as effective tools in the micron and sub-micron regime of machining are well documented. No other process has provided a viable alternative to lasers in terms of quality or economy of production. However, improvements are needed in reducing the size and taper of features and minimize collateral thermal damage. Shorter pulse widths have proved to be capable of reducing formation of HAZ by reducing the interaction time of the laser with the material during machining. This essentially reduces the 'dumping of heat' into the lattice structure of the material. The development of ultrafast lasers has given laser-processing capabilities a totally new dimension. These lasers possess pulse widths smaller than 1 picosecond, which essentially translates into very high intensities acting on the material for an extremely short time. Improvements in feature definitions have been observed even in materials not given to ease of mechanical processing.

Biomedical components and devices have stringent control on their properties and specifications. Invasive devices like catheters and balloons have to be surgically 'clean' to prevent complications in the human body. However these devices require advanced mechanical processing to enhance their capabilities, but such processes suffer from low throughput. Conventional lasers (Nd: YAG and excimer lasers) also suffer from inherent drawbacks of poor taper control and formation of HAZ. These defects are totally unacceptable to the medical device industry. Ultrafast lasers were considered to investigate their superior material processing capability with respect to biomedical devices.

Optical components including solid lenses are an integral part of any laser system. Research and subsequent advances in microscopy and optical materials have produced lenses possessing wide capabilities and applications. Concepts of linear refractive index and Kerr nonlinear liquids have been investigated in detail previously. The nonlinear property of certain liquids make them intensity dependent which essentially causes to act like a lens or a self focusing medium under a sufficiently intense light. Investigations into laser-liquid interactions helped us formulate liquid lenses capable of performing micromachining. The effects of these lenses on different materials were studied.

Diamond, has been of widespread use because of its several unique and extreme properties. These include but are not limited to the highest hardness, the highest thermal conductivity, chemical stability, refractive index and elastic modulus. A combination of these properties makes diamond a highly desirable material for various applications, which include cutting tools, thermal spreaders and microelectronic devices because of its very high band gap. However, on the downside, the extreme physical properties of diamond or specifically its hardness makes mechanical processing difficult and uneconomical; its high sublimation point makes it unyielding to thermal processes; and its high optical band gap makes even laser processing infeasible. This report studies the ultrafast laser interactions with Type IIa diamond, which is one of the most optically pure diamonds. Its optical purity makes it harder to machine using conventional lasers and this observation was investigated in this work.

Thesis Organization

The thesis is organized into four chapters and one Appendix. Chapter 2 provides a background to previous research into ultrafast lasers and nonlinearity in terms of laser processing. Chapter 3, a paper published in Applied Physics Letters, deals with investigations into the feasibility of using nonlinear liquids as lenses. Chapter 4, a paper accepted for publication in ASME's Journal of Manufacturing Science and Engineering, presents results on the ultrafast laser processing of Type IIa diamond. An analytical model calculated electron temperatures and predicted ablation depth per pulse. Chapter 5 summarizes the major conclusions and suggests work for future development and research. Appendix A presents results and observations from an investigative study of application of femtosecond lasers in the biomedical device industry.

CHAPTER 2. LITERATURE REVIEW

Dyer[1] was one of the earliest to extensively document the unique properties of diamond in 1967. The paper discusses essential characteristics of diamond, including, its chemical composition, crystal structure and more importantly the various types of diamond available. This thesis has reported investigations on Type IIa diamond. These diamonds are practically pure of nitrogen impurity and constitute just 2% of all naturally produced diamonds. Because of their high purity, this type of diamond has excellent thermal and optical properties.

Conventional machining of diamond has involved using grinding wheels charged with diamond grit or powder. Advances have included bonding the diamond to metal alloys or resins to the wheel for additional stability. However, conventional grinding has to factor in the crystallographic orientation of diamond. Overheating of the diamond could result in irreversible damage, as diamond is unstable at higher temperatures.

Non-traditional methods of machining diamond have been developing for some time. These methods typically work on a non-contact process to prevent damage to the diamond crystal. Ion beam assisted etching of diamond[2] achieves etch rates of approximately 20 picometer/min. However, the method introduces contaminants in the processed crystal[3].

Laser machining of diamond

Since the development of lasers, there have been rapid advancements in the areas of laser applications. Lasers have been used rather extensively to machine diamond. Some of

the earliest work on laser machining was performed using Nd: YAG lasers[4], the most preferred laser for machining diamonds. Nd: YAG lasers typically are used in the 1.06 μm regime. However, Type IIa diamond is virtually free of nitrogen, which makes it highly transparent. Nitrogen imparts enhanced absorption capability to diamond. It was demonstrated by Douglas-Hamilton[5] that CO_2 lasers with a fluence of 10^6 J/cm^2 was unable to machine the diamond because of its optical transparency.

Conventional laser processing has its drawbacks. Due to the low absorption characteristics of diamond, higher than normal laser fluences are employed. However, the longer pulsewidths of the lasers have deleterious effects on the material properties and microstructure, which are undesirable. The development in the field of ultrafast laser technology has brought a new dimension to the area of diamond machining. A typical ultrafast laser has a pulsewidth shorter than 1 picosecond with incident intensities of a few terawatts. Also, most ultrafast lasers operate in the ultraviolet to infrared wavelengths.

Femtosecond laser theory

The generation of femtosecond pulses is achieved predominantly by mode locking. Rulliere[6] reported that a laser cavity has multiple modes oscillating simultaneously. Due to the randomness of their phase differences, the intensity also shows a random time distribution. However, if it were assumed that the phase differences between the modes were constant, the laser output would consist of periodic succession of single pulses. Each pulse would last $\Delta\tau$ and the repetition rate would be given by $T = 2L/c$ where $\Delta\tau$ is the pulsewidth, L the length of the resonator cavity and c the speed of light. The laser is then supposed to be mode locked. Ti: sapphire lasers are currently one of the most common

group of ultrafast femtosecond lasers. This specific laser has the advantage of being easily mode locked by either the introduction of an acousto-optical crystal or by pumping the medium with another mode-locked laser.

The high intensities associated with ultrashort pulses have inherent problems. These problems are associated with the nonlinear problems of intense light as reported by Marjoribanks[7]. Some of these problems include

- B-integral problems

This problem is associated with the dependence of the index of refraction of light on the intensity. Thus a beam with a non-uniform intensity distribution (Gaussian profile) passing through a window of glass or even a distance of air suffers a delay of phase at the center of the beam which differs from that at the beam edges. This alteration of phase causes distortion, which can lead to significant problems during focusing. Some of them are explained below

  - Self focusing

  Differences in optical path lengths as introduced by a lens lead to the introduction of delays in certain phases. This leads to the collapse of the whole beam or a part of it to a focus even within the laser rod itself leading to significant or total destruction of the system.

  - Filamentation

  Filamentation is similar to the phenomenon explained above. The difference between the collapse of the whole beam and its parts is the relative growth rates of individual spatial-frequency components.

- Self-phase modulation

Similar phase distortions can cause the light to be optically chirped. Changing intensities of a pulse of light cause leading edges of 'weak' light to add to the period between phases causing reduction in frequency or it might reduce optical period causing an increase in frequency. A pulse containing variable frequencies is said to be optically chirped.

- Nonlinear optical damage

The maximum power or fluence of a laser system may be limited by the small absorption of laser energy by components of the laser system. This leads to a damage threshold for laser mirrors and other components, which causes irreparable damage to the components. This damage is dependent on the wavelength and duration of the laser pulse.

Chirped-pulse amplification

In high power short pulse laser systems, peak intensity is responsible for damage to laser components and systems. The CPA technique[8] reorders laser pulses based on their frequency components into a time-stretched lower intensity peak of equal energy. This lower intensity pulse is safely amplified to a high energy and reconstituted back to a short pulse of very high peak power. Diffraction gratings in matched pairs are used to accomplish this optical phenomenon. One set of gratings called a 'stretcher' causes the pulse to arrive at different time ordered by frequencies. The other complementary set of gratings called a 'compressor' reproduce the pulses almost exactly to the original high intensity. It should be noted that the compressor is arranged in such a way that the amplification of the pulse is completed before rearrangement. The CPA technique is

universally used for femtosecond pulse generation in lasers. Figures 2.1 and 2.2 illustrate the CPA technique.

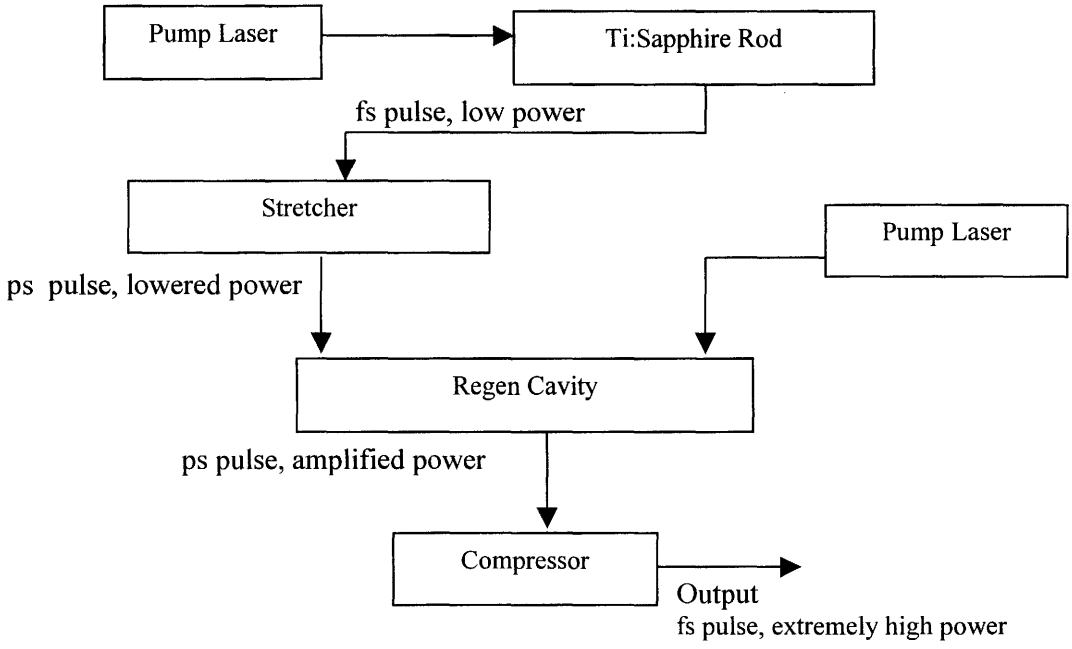

Figure 2.1 Schematic of CPA technique

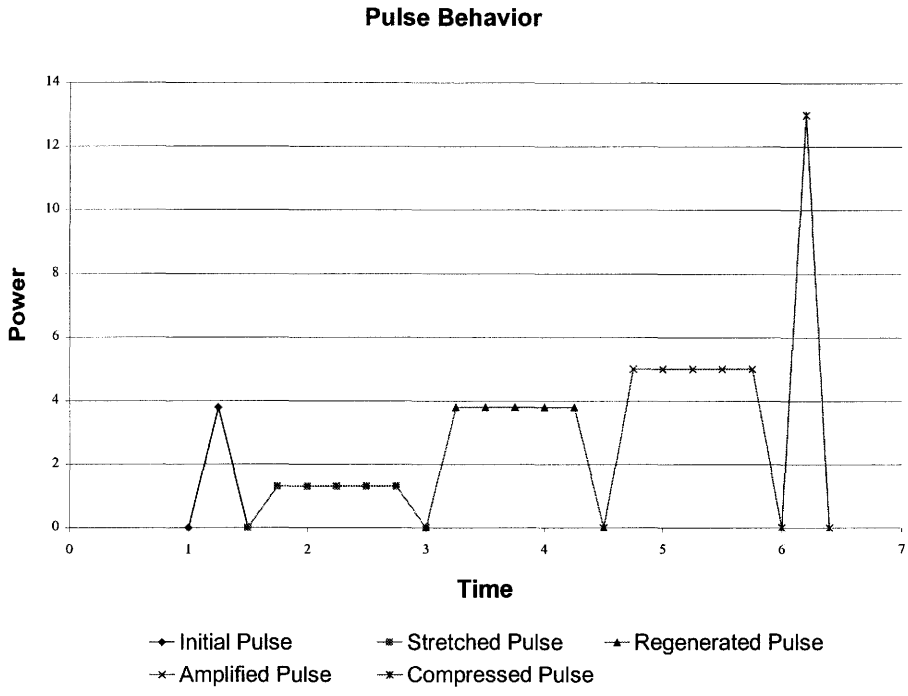

Figure 2.2 Illustration of pulse behavior

Femtosecond pulse machining of materials

Since the inception of ultrafast lasers, considerable research has been carried out to investigate the capabilities of these lasers. Linde[9] explains some of the physical mechanisms behind short pulse laser ablation. He demonstrated that removal of material from the surface of metals and semiconductors occurs on a nanosecond timescale following ultrafast pulses. Lenzner[10] conducted ablation experiments with sub-10 fs laser pulses in several glasses. Their investigations reported potential for lateral and vertical machining precision of the order of 100 nm. Momma et. al[11] conducted specific experiments with a 150-fs Ti: sapphire laser on solid targets. They also compared the results with nanosecond

pulses and demonstrated the superiority of the shorter pulses. An important discussion in their work describes that the effective ablation depth was greater than the optical penetration depth. Analytical modeling on the laser ablation mechanisms of femtosecond laser ablation was completed and qualitative explanations were given about the difference from picosecond and nanosecond pulses[12].

Nonlinear Liquids and their Applications

Nonlinearity has been an area of research in the field of laser applications. The intensity dependence of nonlinearity is particularly relevant in terms of lasers because of their highly coherent and intense light. Early work by Chiao[13] reports self-trapping of optical beams. The discussions included conditions under which, an electromagnetic beam can produce its own waveguide and propagate without spreading. The conditions include materials whose dielectric constant increases with field intensity. Kelley[14] studied a situation where the self-focusing effect due to increasing nonlinear index is not counteracted by diffraction. Numerical analysis of the nonlinear wave equation yields self-focusing length, defined as the distance in which the intensity of the self-focused region tends to become very high. Akhmanov[15] determined conditions required for the nonlinear medium to produce a focusing effect on the beam. Sacchi[16] has extensively studied the phenomena of self-focusing and self-trapping of laser beams. The work gives numerical analysis to determine simplified relations for calculation of self-focusing distance. The author also studied experimentally filament diameters, duration and spectral properties of the filaments.

Recent studies have been more focused on the physics of the phenomenon of laser interactions with nonlinear media. Said[17] reported measurements of nonlinear indices. A single beam experimental technique was used to plot transmittance through an aperture to calculate nonlinear refractive index. The method employed both continuous wave CO_2 and pulsed Nd: YAG lasers.

References

1. Dyer, H.B. 1967. Physical and mechanical properties of diamond. *Proceedings of Industrial Diamond Conference* I to VIII.
2. Rothschild, M., C. Arnone, D.J. Ehrlich. 1986. Excimer-laser etching of diamond and hard carbon films by direct writing and optical projection. *J. Vac. Sci. Technol.* B 4(1), 310-314.
3. Malshe, A.P., S.T. Kshirsagar, K.S. Chari. 1991. Excimer laser-induced etching of non-hydrogenated (a-C) and hydrogenated (a-C:H) diamond-like carbon films: a comparative study. *Materials Letters* 11(5,6,7), 175-179.
4. Gresser, D. Herbert. 1976. Laser sawing of diamonds. *Society of Manufacturing Engineers.* Technical paper MR76-855.
5. Douglas-Hamilton, D.H., E.D. Haag 1974. Diamond as a high-power laser window. *J. of the Optical Soc. Of America.* 64(1), 36-38.
6. Ducasse, A., C. Rulliere, B. Couillaud. 1998. Methods for the generation of ultrashort laser pulses: Mode locking. *Femtosecond Laser Pulses*. C. Rulliere ed. Springer Verlag Germany.
7. Marjoribanks, R. S. 2000. Chirped pulse amplification lasers. Updated July 2000. http://www.physics.utoronto.ca/~marl/CPAgen.html
8. Strickland, D., and G. Mourou 1985. *Optical Communications.* 56: 219-224
9. Linde, von der D., K. Sokolowski-Tinten 2000. The physical mechanisms of short pulse laser ablation. *Appl. Surf. Sc.* 154-155 1-10.

10. Lenzner, M., F. Krausz, J. Kruger, W. Kautek. 2000. Photoablation with sub-10 fs laser pulses. *Appl. Surf. Sc.* 154-155 11-16.
11. Momma, C., S. Nolte, B.N. Chichkov, F. v. Alvensleben, A. Tunnerman. 1997. Precise laser ablation with ultrashort pulses. *Appl. Surf. Sc.* 109/110 15-19.
12. Chichkov, B. N., C. Momma, S. Nolte, F. v. Alvensleben, A. Tunnerman. 1996. Femtosecond, picosecond and nanosecond laser ablation of solids. *Appl. Phys. A.* 63 109-115.
13. Chiao, R. Y., E. Garmire, C. H. Townes. 1964. Self-trapping of optical beams. *Phys. Review Lett.* 13(15) 479-482.
14. Kelley, P. L. 1965. Self-focusing of optical beams. *Phys. Review Lett.* 15(26) 1005-1008.
15. Akhmanov, S. A., A. P. Sukhorukov, R. V. Khokhlov. 1966. Self-focusing and self-trapping of intense light beams in a nonlinear medium. *Sov. Phys. JETP.* 23(6) 1025-1033.
16. Sacchi, C. A. 1976. Self-focusing and self-trapping of intense laser beams. *Lasers and their Applications.* Ed. A. Sona. Gordon and Breach. 561-578.
17. Sheik-bahae, M., A. A. Said, E. W. van Stryland. 1989. High-sensitivity, single beam n_2 measurements. *Opt. Lett.* 14(17) 955-957.0

CHAPTER 3. LASER MICROMACHINING USING LIQUID OPTICS

A paper published in Applied Physics Letters

Diwakar Ramanathan[1] and Palaniappa A. Molian[2]

Abstract

Lasers are well suited for micro manufacturing by ablating nearly all the material within the focal spot before any significant heat conduction or mass flow takes place, thus enabling precise machining with little thermal damage. In this letter, the results of a novel idea of using nonlinear liquids as lenses to fabricate micron-sized features are reported. Our research showed that transmitting the laser pulse through a transparent condensed medium such as carbon disulfide that has very high intensity-dependent nonlinear refractive index creates a lens and focuses the beam. Results on 316 stainless steel showed a two-fold decrease in the hole size, and reduced taper when liquid optics were used over traditional solid optics. Polarization effects were also substantially reduced. The beneficial effects of liquid optics are explored.

Introduction

Micromachining is an important technology that has both immediate and future applications in diverse fields such as microelectronics, photonics, high-density magnetic recording, optics, medicine, sensors and actuators (MEMS).

---

[1] Primary researcher and author.
[2] Major Professor and author for correspondence.

Lasers have been proven as effective tools for micromachining [1-5]. With the advent of ultrafast lasers, laser technology has potential to surpass the competing technologies of electrodischarge machining and focused ion beam machining for microstructuring at dimensions less than 1 μm. Lasers are suitable for applications that demand more precision, speed, automation, and "direct write" capability. The attributes of laser micromachining include excellent edge quality and reduced heat-affected-zone. Lasers can also work on most materials and are environmentally friendly. Q-switched Nd: YAG and excimer lasers are widely used for micromachining applications that include photoablation, chemical etching, lithography, and surface cleaning. For example, it is now commonplace to create *via* holes as small as 10 μm in polyamide dielectrics for electronic packaging. The benefits of these lasers are attributed to high energy per pulse and nanosecond (ns) pulse widths that allow the beam to strongly interact with materials. Spot size is the governing parameter for obtaining the smallest feature. Clearly, there is a limit to which spot size can be reduced by controlling the optics (focal length and spherical aberration) and beam quality (transverse electromagnetic mode, TEM). Physical optics indicates that if the focal length of the lens is reduced to obtain small spot size, spherical aberration becomes dominant and enlarges the spot size. It is also difficult to find a laser with a perfect TEM_{00}. An alternative method to produce the small spot size is to insert a limiting aperture in the laser beam. However, the loss of power drastically reduces the intensity and renders the process ineffective. Additionally, there is an increase in beam divergence. The current practice is to achieve a small spot in lasers by controlling the intensity profile in such a way that only a fraction of the spot size is above threshold energy fluence (Figure 3.1).

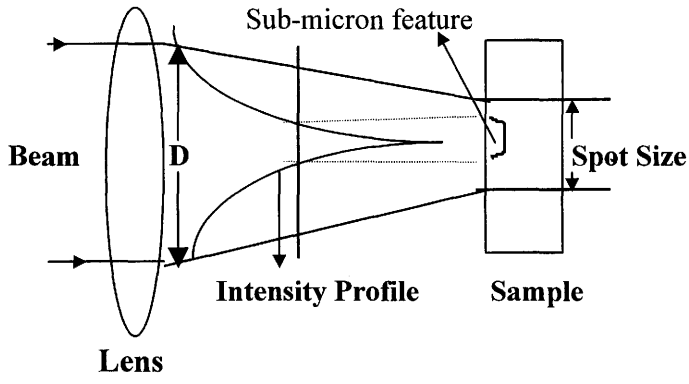

Figure 3.1. Small structures produced by traditional method.

In this way, researchers[6-9] have demonstrated that the machined feature size can be smaller than the spot size. For example, a 60-fs laser with a 5-μm focused spot could produce an 800-nm hole in SiO_2 [7]. Similarly, 300-nm diameter holes were drilled in silver films using a 200-fs laser focused to a spot size of 3-μm[8]. Another example is the creation of 500-nm diameter holes in copper and silicon using a 500-fs laser[9]. The chief limitations of this technique are very low material removal rates due to low energy availability and the difficulty in controlling the feature size. New methods must be sought to reduce the focused spot size without compromising the energy fluence. In this paper, a new method using nonlinear liquid is attempted to generate small spot and then applied to fabricate precision holes. The approach is based on the optical effects of nonlinear liquids that include self-refraction effects of the pulse beam propagation through transparent condensed media.

When an intense laser beam travels through transparent condensed media (nonlinear liquids), several nonlinear effects are produced. These effects include harmonic and

continuum generation (frequency multiplication and large bandwidths), parametric processes (waves interacting at several frequencies), and self-action (self-focusing and self-trapping effects). We focus on the self-action capability of optical nonlinear liquids to control the spot size. A large body of theoretical and experimental work has been developed on the physics of self-focusing of laser light (using Ruby, Q-switched Nd: YAG, mode-locked Nd: Glass, and Ti: sapphire) in nonlinear liquid media ranging from CS_2 to Chinese tea[10-20] but none have been demonstrated for machining applications. Self-focusing phenomenon (lens effect), explained below, is attributed to the clustering of molecules, anisotropy, electron distortion, orientation of asymmetric molecules in the presence of strong optical fields, and size of molecules.

When an intense laser beam propagates through a nonlinear, condensed medium whose refractive index increases with field intensity, it creates its own optical waveguide and transmits without diffraction spreading. The refractive index of the condensed medium (n) is the sum of the linear refractive index of the medium (n_0) and the refractive index change (δn) which the laser field induces: $n = n_0 + \delta n = n_0 + n_2 |E|^2$ where n_2 is the nonlinear refractive index and E is the amplitude of the electric field. Since the laser beam has an inherently non-uniform intensity distribution, the intensity-dependent index of refraction (δn) causes different parts of the beam to propagate with different phase velocities. A lens effect is thus produced whereby the rays move toward the region of higher intensity, reducing the spot size (Figure 3.2). Thus, self-focusing is an inductive lens effect resulting from the lopsided changes of the action of the laser wavefronts themselves, and thus the liquid acts as a convergent lens with a focal length (f) given by [12]:

$$f = (n_0 / \delta n)^{1/2} (D/2E)$$

The self-focusing effect will obviously be counteracted by the beam diffraction, which is the spread of a beam of finite cross-section over distance. Therefore, it is possible that the two effects will compensate each other at a distance called self-focusing distance (l) after which extremely small spots may be produced. "l" may be obtained by numerically solving the non-linear wave equation. The self-focused beam has a diameter two-orders of magnitude smaller than the focal diameter [10,11] as observed in laser beams transmitted through CS_2 and nitrobenzene at threshold power. The spot size continues to decrease with increased intensity. Another interesting characteristic of the beam propagation through liquids is dynamic focusing [19]. That is, the pulse does not focus to single, small foci but rather to a moving focus along the optical axis. This will reduce the taper and possibly assist

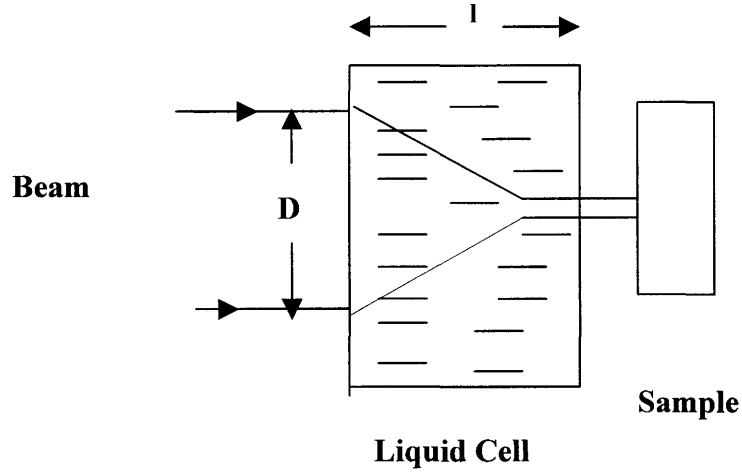

Figure 3.2. Small structures produced by present method.

in machining thicker sections. Multiple holes can also be generated with a single beam especially at higher intensities because of the small-scale focusing [18] that breaks the beam into numerous filaments and due to the presence of group velocity dispersion in the medium[17, 20] that splits the original pulse.

Materials and Methods

The sample used in this work was 316 stainless steel with a thickness of 0.1 mm. The sample was thoroughly cleaned in methanol, mounted on a computer controlled x-y stage and secured. A 15-nsec pulsed Q- switched Nd: YAG laser was used to process the steel. The specifications of the laser include 1064 nm wavelength, 400 mJ pulse energy, 10 Hz repetition rate, 4 mm beam diameter and linear polarization. A 150-mm focal length solid lens was used to focus the beam at the sample to a size of about 1.3-mm. The laser was operated at a repetition rate of 1 Hz for the experiments. Drilling was performed in air at ambient temperature and pressure. Pulse energy and number of pulses were varied to obtain through-holes.

A survey of different organic and inorganic liquids indicates that the most promising nonlinear liquids (liquid optics) are carbon disulfide and benzene. Table 3.1 lists the optical properties and the self-focus characteristics of these liquids. CS_2 requires lower powers for self-action than other liquids because large groups of molecules create high optical density thereby increasing the nonlinear refractive index.

Table 3.1. Optical, self-action, continuum and energy loss properties of selected nonlinear liquids.

Liquid	**Linear Refractive Index, n_0 (esu)**	**Nonlinear Refractive Index, n_2 (esu)**	**Continuum Bandwidth, nm**	**Energy losses (%)**
Benzene	8.5×10^{6}	54×10^{-12}	780-810	<1
Carbon disulfide	9.0×10^{6}	96×10^{-12}	795-805	<1

The critical power needed to self-focus the beam is given by [12],

$$P_{cr} = 0.0032 \, (\lambda^2 \, C / n_2)$$

where, λ = wavelength of the laser beam (m), C = speed of light in vacuum (m/s), n_2 = nonlinear refractive index. The critical power for self-focusing is calculated to be 11.32 kW.

Energy losses associated with absorption and scattering are very low, too. In addition to these two liquids, other nonlinear liquids including acetone, methanol, sodium chloride and ammonium chloride were tested under similar processing parameters.

Figure 3.3 shows a schematic of the experimental setup for the liquid optics. Because of its low absorption characteristics, a quartz beaker was used to contain the liquid. The height of the liquid column was about 16 mm.

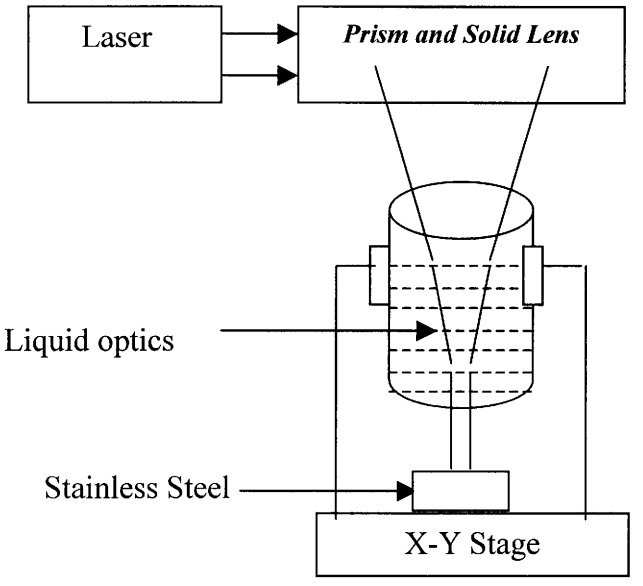

Figure 3.3 Experimental setup for nonlinear liquid assisted laser drilling.

The self-focusing length 'l' was calculated using the following relation[21],

$$l = (d/2)\,[n_o/(2\,n_2\,Io)]^{0.5}$$

where, d = beam diameter (m), n_o = linear refractive index (esu), n_2 = non-linear refractive index (esu), I_o = maximum intensity (W/m^2). The self-focusing distance was calculated to be 40 mm.

The gap between the liquid and the sample was kept constant at 4 mm. The gap was made small to minimize the divergence of the beam after emerging from the liquid cell. The spot size at the liquid surface was calculated to be 1.67-mm. Energy measurements at various points along the beam travel path were made to find the losses due to the insertion of the liquid in the laser beam path. The measurements showed that less than 1 % of the beam energy was lost. The energy of the laser beam was varied along with number of pulses. The samples were then examined in a scanning electron microscope (SEM, Model JEOL 840A)

operating at 10-kV accelerating voltage. Secondary electron images were generated to obtain information on the feature size, shape, recast layer, and cracks formation.

Results indicated that the most promising liquid was CS_2. Other liquids had either marginal or deleterious effects on the size, taper, recast layer and heat-affected zone. Figure 3.4 shows the effects of solid and CS_2 liquid optics on the hole dimensions. The exit hole diameters are also plotted on the same curve to give an indication of the taper. The holes with the liquid optics were obtained using a single pulse while the holes with the solid optics were produced with the number of pulses varying from 4 to 8. Figure 3.4 demonstrates the effectiveness of liquid optics in producing small feature and minimizing taper.

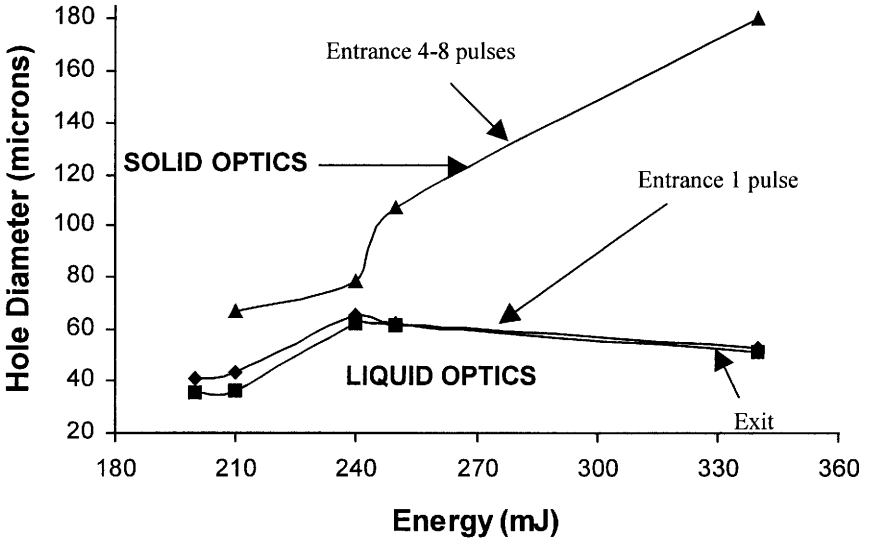

Figure 3.4. Variation of hole diameter with pulse energy for solid and liquid optics.

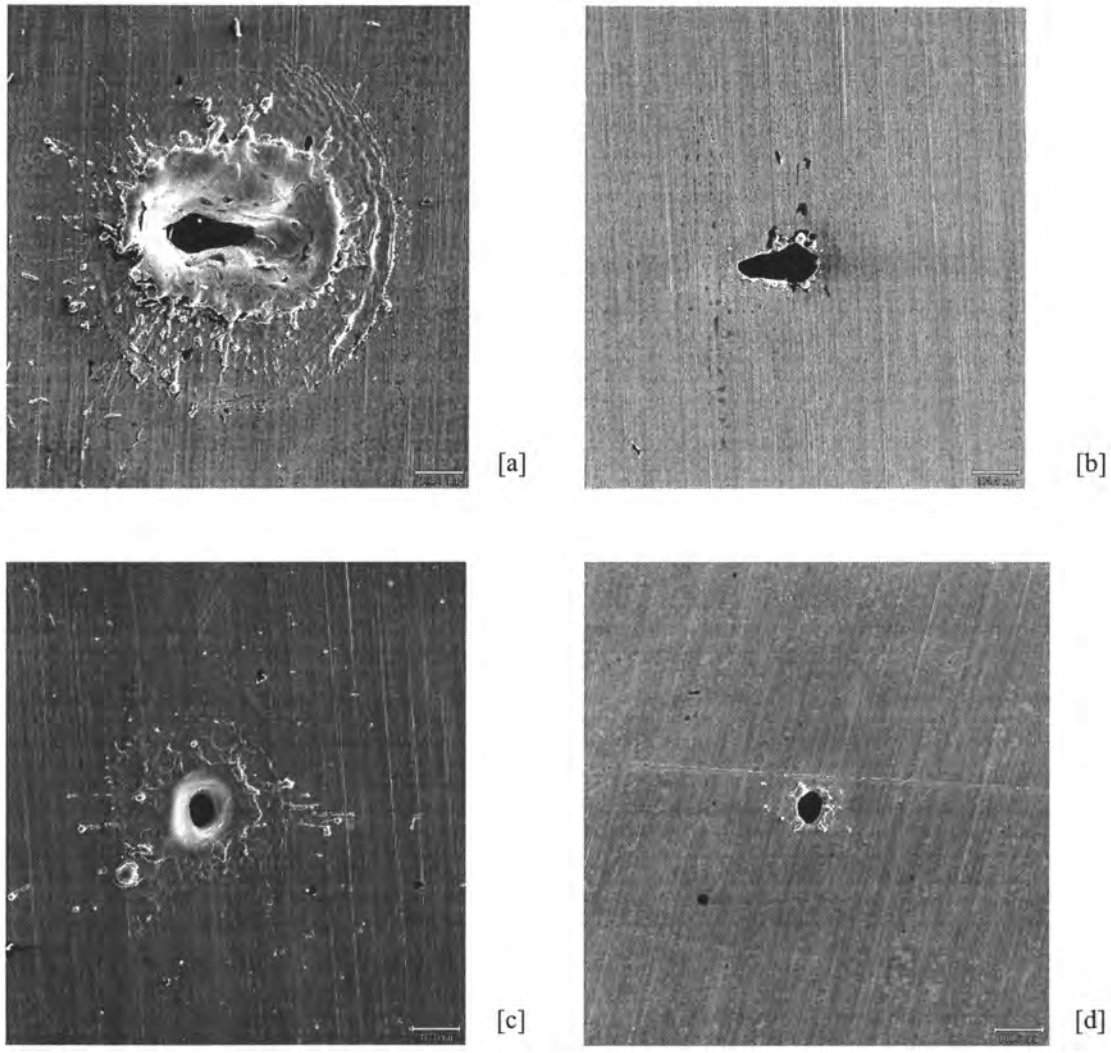

Figure 3.5 SEM micrographs showing entrance and exit holes for solid (a) and (b) and liquid (c) and (d) optics at 80x magnification.

Figure 3.5, SEM micrographs of holes drilled with solid and liquid optics, shows the improved edge definition and minimal recast layer/HAZ for the holes drilled using the liquid optics. The holes drilled with the solid optics were distorted in shape due to the linear polarization of the Nd: YAG beam. Nevertheless, the liquid optics has reduced the polarization effects. In addition, the number of pulses required to drill through the sample with liquid optics is much less than that required with solid optics. Preliminary research has proven that there is a marked improvement in producing finer holes with improved quality by using nonlinear liquid optics.

The authors would like to acknowledge the National Science Foundation (NSF) for supporting this research work under the grant DMI – 9978633.

References

1. Resonetics, Inc., "Resonetics illustrated guide to laser applications micromachining," http://www.resonetics.com/applications.shtml
2. Oxford Lasers, Inc.,"Laser-based micromachining," http://www.oxfordlasers.com/MP.html
3. Potomac Technology, Inc., "Laser processing works on a micro scale," http://potomac-laser.com/technology/micro.html
4. Louisiana Tech., "Laser ablation examples," http://www.latech.edu/tech/engr/if...laser/laser_ablation_examples.htm
5. S.C. Hennink, "Machining lasers find niches by solving very small problems," Photonics Spectra 116-118 (November 1997).
6. M.D. Shirk and P.A. Molian, "A review of ultrashort pulsed laser ablation of materials," J. of Laser Appl., 10 (1), 1-11 (1998).
7. X. Liu and G. Mourou, " Ultrashort laser pulses tackle precision machining," Laser Focus World, 101-118 (August 1997).

8. P. Pronko, S. Dutta, J. Squier, J. Rudd, D. Du and G. Mourou, " Machining of submicron holes using a femtosecond laser at 800 nm," Opt. Comm., 114, 106-110 (1995).
9. P. Simon and J. Ihlemann, "Machining of submicron structures on metals and semiconductors by ultrashort UV-laser pulses," Appl. Phys. A 63, 505-508 (1996).
10. S.A. Akhmanov, A.P. Sukhorukov and R.V. Khokhlov, "Self focusing and self trapping of intense light beams in a non linear liquid medium," Soviet Physics JETP 23 (6), 1025-1033 (December 1966).
11. R. Brewer, J.R. Lifsitz, E. Garmire, R.Y. Chiao and C.H. Townes, " Small-scale, trapped filaments in intense laser beams," Phys. Rev. 166 (2), 326-332 (1968).
12. C. A. Sacchi, "Self-focusing and self trapping of intense laser beams," Lasers and their Applications edited by A. Sona (Gordon and Breach, New York, 1976), pp-561-578.
13. A. Ashkin, J.M. Dziedzic and P.W. Smith, " Continuous-wave self focusing and self trapping of light in artificial Kerr media," Optics Letters 7(6), 276-282 (1982).
14. A. Drobnik, "On the certain results of the laser light with various media," SPIE 1391, Laser Technology III, 211-213 (1990).
15. P.P. Banerjee, R.M. Mishra and M. Magharaoui, "Theoretical and experimental studies of propagation of beams through a finite sample of a cubically nonlinear material," J. Opt. Soc. Am. B 8(5), 1072-1080 (1991).
16. M. Mitchell, M. Segev, T.H. Coskun and D.N. Christodoulides, "Theory of self-trapped spatially incoherent light beams," Phys. Review Letters 79 (25), 4990-4993 (1997).
17. A. Brodeur and S.L. Chin, "Bandgap dependence of the ultrafast white-light continuum," Phys. Review Letters 80(20), 4406-4409 (May 1998).
18. A. Brodeur, F.A. Ilkov and S.L. Chin, "Beam filamentation and the white light continuum divergence," Opt. Comm. 129, 193-198 (1996).
19. D. Strickland and P.B. Corkum, " Resistance of short pulses to self-focusing," J. of Opt. Soc. of A. 11(3), 492-497 (March 1994).
20. J.E. Rothenburg, " Pulse splitting during self-focusing in normally dispersive media," Optics Letters 17(8), 583-585 (April 1992).
21. P. Lallemand and N. Bloembergen, " Self-focusing of laser beams and stimulated Raman gain in Liquids," Phys. Review Letters 15(26), 1010-1012 (1965).

CHAPTER 4. MICRO- AND SUB-MICROMACHINING OF TYPE IIa SINGLE CRYSTAL DIAMOND USING A Ti: SAPPHIRE FEMTOSECOND LASER

A paper to be published in ASME Journal of Manufacturing Science and Engineering in May 2002

Diwakar Ramanathan[1] and Palaniappa A. Molian[2]

Abstract

A 200-fs pulsed Ti: Sapphire laser was used to micromachine Type IIa single crystal diamond. The effects of the pulse energy and exposure time were investigated. Both blind and through holes were generated by trepanning and percussion modes. Trenches were produced by the direct-writing mode. Scanning electron and atomic force microscopy analysis revealed that the holes are in the range 0.65-100 μm and are free from taper. In addition, there was little recast layer around the holes. The damage threshold was approximately 4 J/cm^2, which is smaller than those obtained from other lasers. A two-temperature model was used to establish the electron temperatures and to predict the ablation depth per pulse. It is evident from this work that femtosecond lasers are capable of producing micro- and sub-micron structures with very high precision.

[1] Primary researcher and author.
[2] Major Professor and author for correspondence.

Introduction

Diamond is the ultimate material in terms of hardness, elastic modulus, thermal conductivity, electrical resistivity and refractive index [1-5]. It is also well known for chemical resistance with the exception of high-temperature oxidation. As semiconductors, doped diamonds exhibit the highest saturated electron velocity, the lowest dielectric constant, the highest dielectric strength, and the largest band gap [1,2]. The characteristics of high wear resistance and low frictional resistance enable diamond as an excellent tool for machining of metal/composites/wood, testing of hardness, cutting optical fibers in telecommunications, and in numerous other hard tooling applications. Dies for wire drawing has been one of diamond's most successful applications. The application areas of diamond in electronics include Single Crystal Diamond (SCD) FETs (Field Effect Transistor) and MOSFETs (Metal Oxide Field Effect Transistors). The very high thermal conductivity and its electrically insulating properties makes diamond an ideal material for computer packaging applications.

Diamonds are classified into four types: Ia, Ib, IIa and IIb depending on the nature, concentration and distribution of the impurity content. Type IIa SCD, chosen in this work, constitutes about 2% of all the production and is virtually free of nitrogen impurity. Consequently, this diamond exhibits superior optical, thermal, and cleavage properties. At room temperature, Type IIa diamond has a thermal conductivity approximately six times that of copper (Type Ia has only two times by comparison) [4]. This characteristic is particularly important when it is used as a tool for machining because heat can be dissipated much faster from the cutting zone thus preventing extreme temperature gradients and subsequent thermal shock. Type IIa diamond serves as a better optical window material than other types [3].

Single-crystal diamond tools are in use because extremely sharp cutting edges and very low friction surfaces are attainable. They are able to impart extremely fine surface finishes to lenses in the optics industry [1].

Rough shaping and cleaning of industrial diamond using Nd:YAG lasers operating in fundamental and second harmonic wavelengths is currently in practice [5]. Recently, ultraviolet, nanosecond pulsed excimer lasers have demonstrated high precision machining of diamond due to its greater absorption by diamond [5]. The excimer lasers have the lowest damage (ablation) threshold fluence compared to other lasers. Femtosecond pulsed laser machining is a recent technology that has potential to produce fine tools and devices (windows, thermal spreaders) in diamond by virtues of multiphoton absorption effects and less thermal diffusion. Femtosecond lasers operating in the 700-850 nanometer wavelength range produce peak powers of over a gigawatt. In this work, a chirped pulse amplification (CPA) Ti: sapphire laser with a pulse width of 200-fs was used for drilling and grooving of Type IIa SCD, the purpose being to produce micro and nanofeatures. Scanning electron microscope (SEM), atomic force microscope (AFM), and Raman spectroscope were used to characterize the features.

Experimental materials and methods

The material used in our investigation was a polished industrial Type IIa single crystal diamond acquired from Harris Corporation (Mount Arlington, NJ). The crystal orientation was [110] and the nominal dimensions of the sample were 3 mm x 3 mm x 0.25 mm. The optical, electrical and physical properties of type IIa diamonds are listed in Table 4.1. Prior to laser processing, the sample was thoroughly cleaned with isopropyl alcohol.

Table 4.1. Properties of type IIa diamond [1-5]

Absorption coefficient	$1.67 * 10^{3}\ m^{-1}$
Density	$3515\ kg/m^{3}$
Specific heat of Diamond	2.0 kJ/kg K
Thermal Conductivity	2600 W/m K
Sublimation Temperature	4000 K

An oscillator-amplifier Ti: sapphire (femtosecond pulsed) laser system based on the chirped-pulsed-amplification (CPA) technique was used for micromachining of diamond. Details on the CPA technique may be found elsewhere [6,7]. The CPA Ti: sapphire laser experiments were carried out at Clark-MXR, Inc., (Dexter, Michigan) using its RG-2001 femtosecond laser workstation. The laser parameters used in this work are listed in Table 4.2. The diamond sample was mounted on a computer-controlled *x-y* table and laser machining was conducted at ambient temperature and pressure. The machining was not assisted by an auxiliary gas jet commonly used in traditional laser machining applications because the debris was expected to be negligible. In addition, diamond machining with lasers is better performed in air to reduce the recast layer because the carbon reacts with oxygen [5]. The variables included pulse energy (63 nJ to 225 μJ), type of machining (trepanning, percussion, grooving), spot size (3 μm and 25 μm) and exposure time (4 ms to 45 min.).

Table 4.2 Laser specifications

Wave length	*Pulse energy	Pulse width	Repetition rate	Beam size	Beam quality	Polarization
775 nm	550 μJ	200 fs	250Hz	6 mm	Near Gaussian	Linear

*Maximum possible at specimen

Figure 4.1 shows the experimental setup of laser micromachining where two optical configurations (80-mm standard focal length lens and 50x-transmission objective lens) were used. Features ranging from 100 μm to less than 1 μm were fabricated on the sample at four distinct regions labeled A, B, C and D. The features processed in A and B are in the 10-100 μm regime and were obtained using a 80-mm focal length that focused the beam on the sample surface to a spot size of 25 μm. Trepanning and percussion methods were used to drill holes in A, while direct writing method was used at a speed of 50 μm/s to machine trenches in B. Lower pulse energies (nJ) and smaller spot sizes (3 μm) were used for regions C and D to obtain very small features (<1 μm). The smaller spot size of 3 μm was achieved using an objective lens of 50x magnification. Only percussion method of drilling was used in regions C and D.

The diamond sample was also processed using a Q-switched Nd: YAG laser (1064 nm, 200 ns) micromachining system (Florod Model MEL 40) for comparison purpose. The pulse energy and spot size were 550 μJ and 25 μm respectively. Following laser processing, four analytical instruments were used to identify, measure and characterize the size, recast layer, crack formation, and chemical contamination of machined regions. A 500X

magnification optical microscope was used to examine the sample for any residual contamination around the machined areas, to locate precisely the various regions and the presence of through holes. The sample was then examined in a scanning electron microscope (SEM, Model JEOL 840A) operating at 10 kV accelerating voltage. Secondary electron images were generated to obtain information on the feature size, shape, recast layer, and cracks formation at various locations. Atomic force microscopy (AFM) was performed using the Nanoscope IIIa Dimension 3000 (Digital Instruments) instrument operated under ambient conditions. All AFM topographic images were collected in the tapping mode by use of a 200-nm tip radius Si_3N_4 cantilever (nanoprobes) with normal bending of 0.12 N/m. All images were acquired using a constant-force mode at a normal force of ~30 nN. A micro-Raman spectroscope was used to identify non-diamond carbon phases possibly from the phase transition of diamond to graphite.

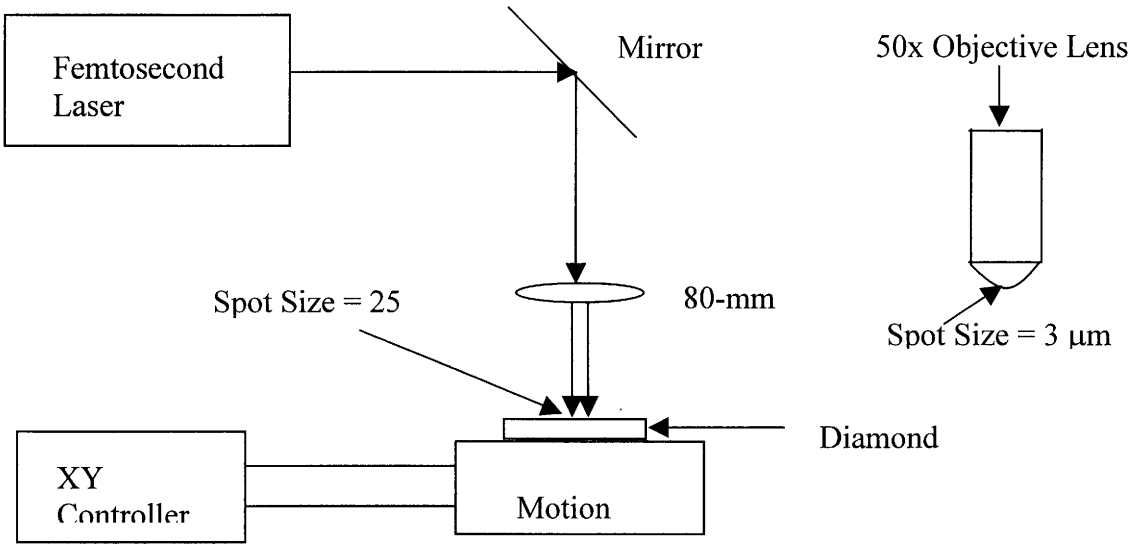

Figure 4.1. A schematic representation of laser micromachining setup

Results

Region A

Table 4.3 shows the femtosecond laser parameters and the resulting hole diameters obtained in region A. Figure 4.2 shows two holes in percussion and trepanning modes that are commonly encountered in laser drilling. Percussion drilling is a stationary process of making holes using multiple pulses where repeated pulsing of focused laser energy at a material creates vaporizing layer by layer until a through hole is "popped". The hole size will be about the same as the focal spot. The absence of relative motion between the laser beam and the workpiece in percussion drilling allows energy to be transmitted to the bottom of the hole by the laser beam being reflected internally off the sidewalls of the hole. In trepanning, holes are produced by first percussion drilling a small hole and then moving either the work piece or the focusing optic by circular interpolation of two axes of motion. Once percussion drilling makes a pilot hole, trepanning is essentially cutting. Trepanning usually generates larger holes than the focused spot diameter. The need to use one method over the other is not always clear, however, when the desired hole size is larger than two times the spot diameter, trepanning must be used. Percussion drilling is the faster process. However, it suffers from poor quality in terms of large taper, re-solidified material at wall of hole, and bellow shape.

Table 4.3 Processing parameters and results for region A.

Hole No.	Drilling Method	Energy (μJ)	Exposure time (min)	Hole Diameter (μm)
1	Trepanning	3	45	54
2	Trepanning	7	15	62
3	Trepanning	22	10	53
4	Trepanning	90	7	58
5	Trepanning	225	7	60
6	Percussion	225	7	17

In the trepanning mode, the hole diameter was made constant at about 60 μm. All these holes were drilled through the sample thickness with almost no taper. The absence of taper is attributed to the ability of femtosecond pulses in minimizing thermal effects. The hole size is much smaller in the percussion mode because the volume of material ablated (kerf) is much larger in percussion than trepanning. Figure 4.2 shows that the holes are much cleaner in the trepanning mode than in the percussion mode. This is attributed to the lower pulse energies and longer exposure times under which conditions the ablation tends to be much more smooth and uniform.

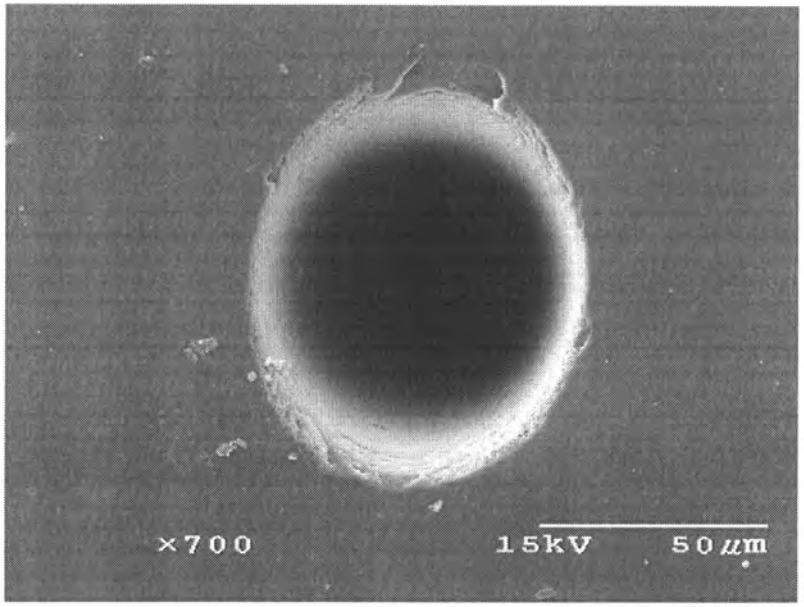

[a]

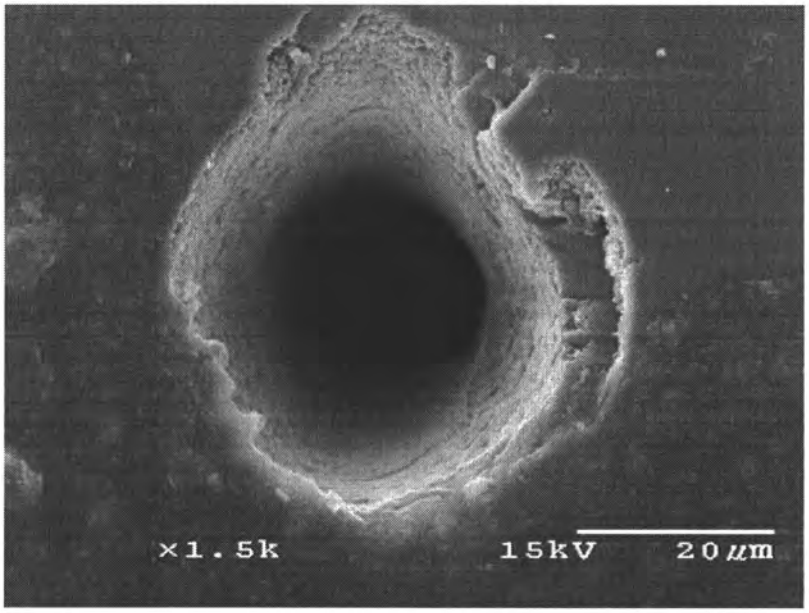

[b]

Figure 4.2 SEM micrographs of holes (a) trepanned (22 μJ, 150,000 Pulses) and (b) percussion drilled (225 μJ, 105,000 Pulses.)

Figure 4.3 shows SEM micrographs of a 200-nanosecond pulsed laser-drilled hole (percussion drilling). The hole size is about the same as that of femtosecond-laser processed hole, however, the hole appears quite distorted. There is clearly pronounced thermal damage and a significant amount of scattered debris. Thermal shocking at the edge of the hole could have generated the 'halo' and the debris around the hole, after which the cracked material was scattered by exiting plasma. The edge definition of the hole is severely degraded. There is a peeling of the surface layers, and less precise boundary around the hole edge. In general, the longer pulse widths cause significant collateral damage observed around the hole.

Figure 4.4 shows the Raman spectra of diamond before and after femtosecond pulsed laser irradiation. No evidence of graphitization or diamond-like carbon formation is observed suggesting that the femtosecond laser ablation is free of "phase-transition". Previous work by Shirk et al.[8] showed that ultra-short pulses were able to eliminate the undesirable ablation products of the longer pulses, and create chemically clean diamond surfaces. Micro-Raman spectra show pure diamond surface, the only difference between the laser ablated surface and the untreated surface is a reduction in the intensity of the peak from 170,000 counts to around 70,000 counts. This could be attributed to the change from a flat planar surface to the slightly rougher surface within the hole. Previous studies have shown significant peak broadening and even elimination of the diamond peak from nanosecond pulsed laser treated surfaces [8,9].

Figure 4.5 shows the exponential relation of exposure time and pulse energy for 60 μm holes in the trepanning mode. The relation between pulse energy and exposure time can

be expressed as $t = 44.67\ E^{-0.4}$ where t is the exposure time in seconds and E is the pulse energy in μJ.

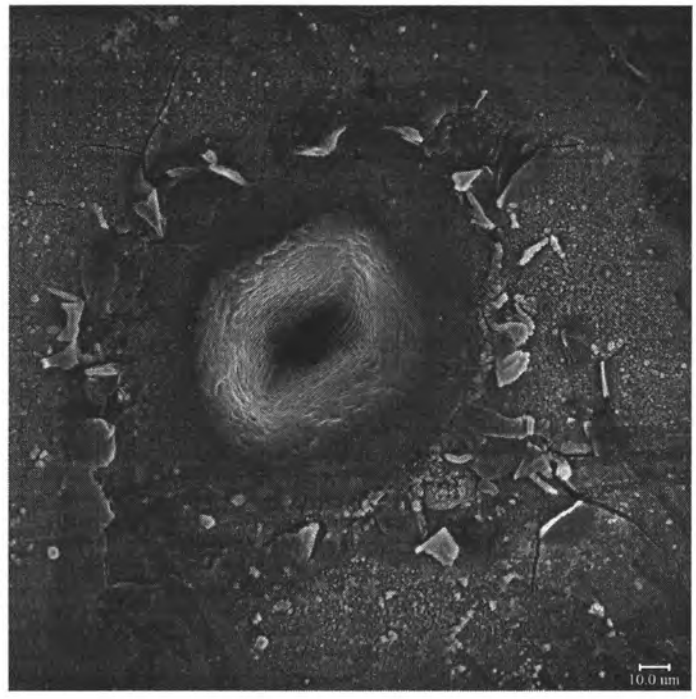

[a]

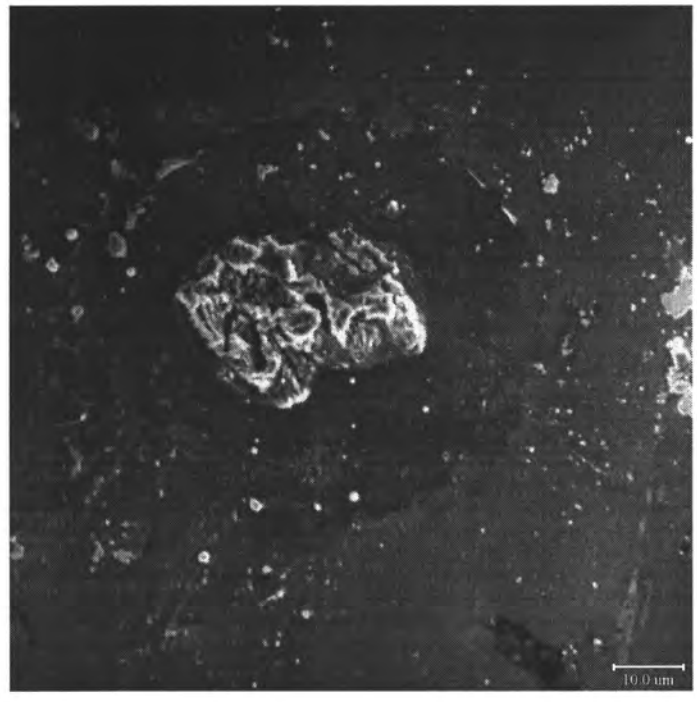

[b]

Figure 4.3 SEM micrographs of the a) front and b) back of a hole drilled by Q-switched, 200-ns Nd: YAG laser.

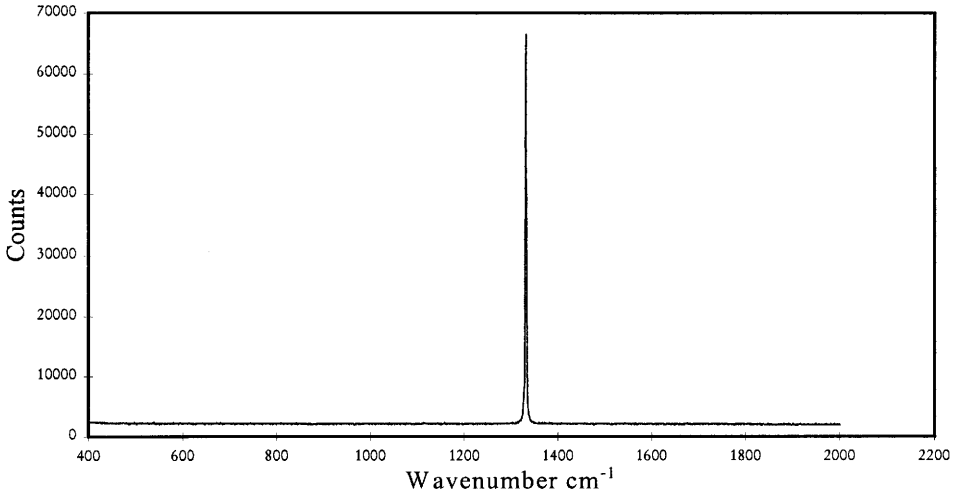

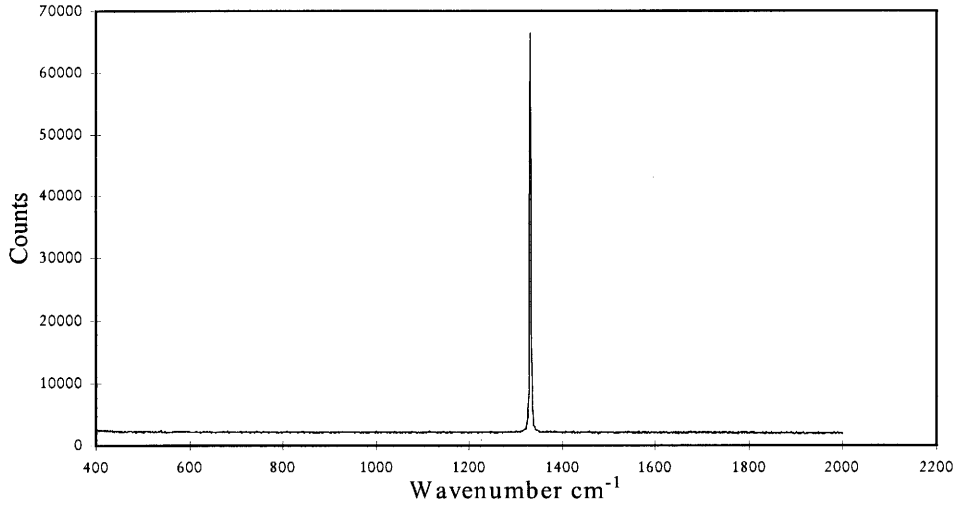

(b)

Figure 4.4. Raman spectra of type IIa diamond surfaces (a) before laser irradiation, (b) after femtosecond laser irradiation.

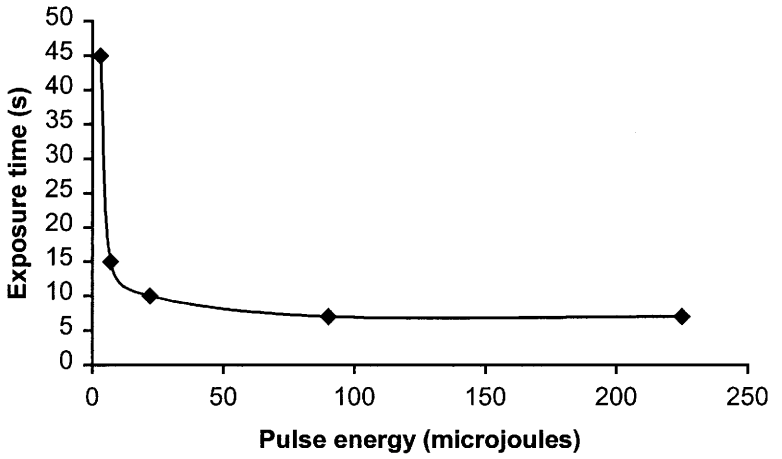

Figure 4.5 Exposure time against pulse energy for trepanned holes.

Region B

Table 4.4 shows the laser processing parameters for the creation of channels in trepanning and percussion modes. The direct writing process was repeated 128 times for each channel. Figure 4.6 shows the SEM micrographs of channels and the absence of contamination. However cracking was observed (Fig. 3.6b) in the trepanning mode at higher pulse energy.

Table 4.4. Processing parameters and results for region B.

Channel #	Drilling Method	Energy (μJ)	Channel Width (μm)
1	Trepanning	45	77
2	Trepanning	90	80
3	Trepanning	225	82
4	Percussion	225	54

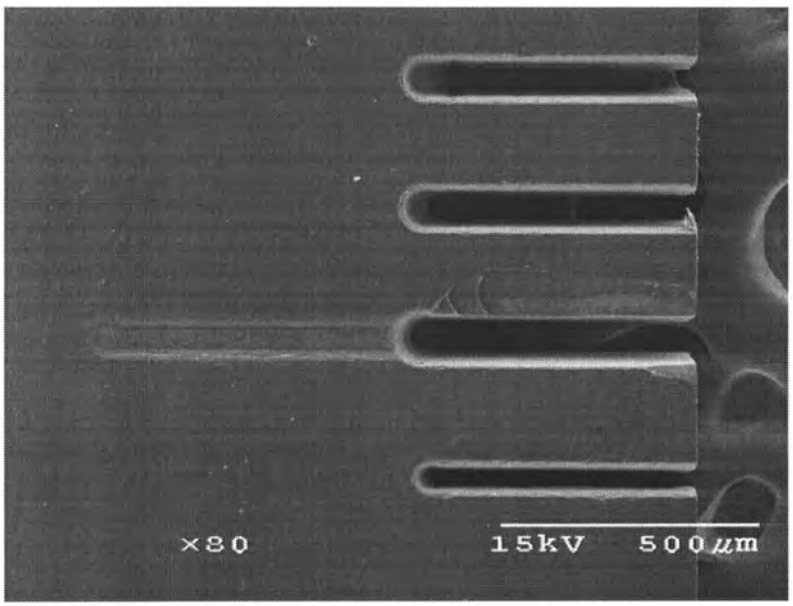

[a]

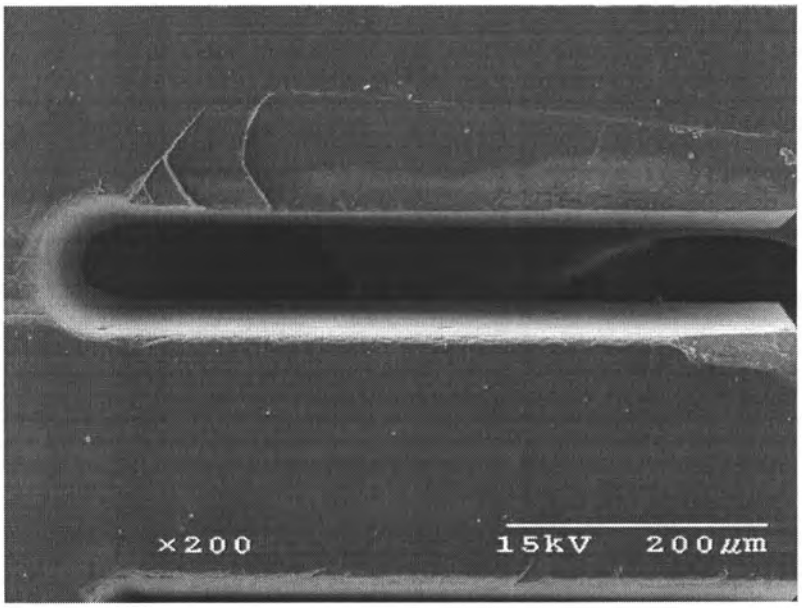

[b]

Figure 4.6 SEM micrographs showing a) Channels (1-4 from top) and b) cracking at Channel 3.

Regions C and D

Pulse energies in the range 200 nJ to 2000 nJ were used to produce holes with diameters less than 1 μm. These holes are extremely clean and show excellent definition with very little evidence of collateral thermal effects. Figure 4.7 demonstrates decreasing feature diameter with decreasing exposure time. Figure 4.8 shows the variation of hole diameter with exposure time (number of pulses). Experiments were also performed using the defocused beam, which generally yielded craters instead of holes.

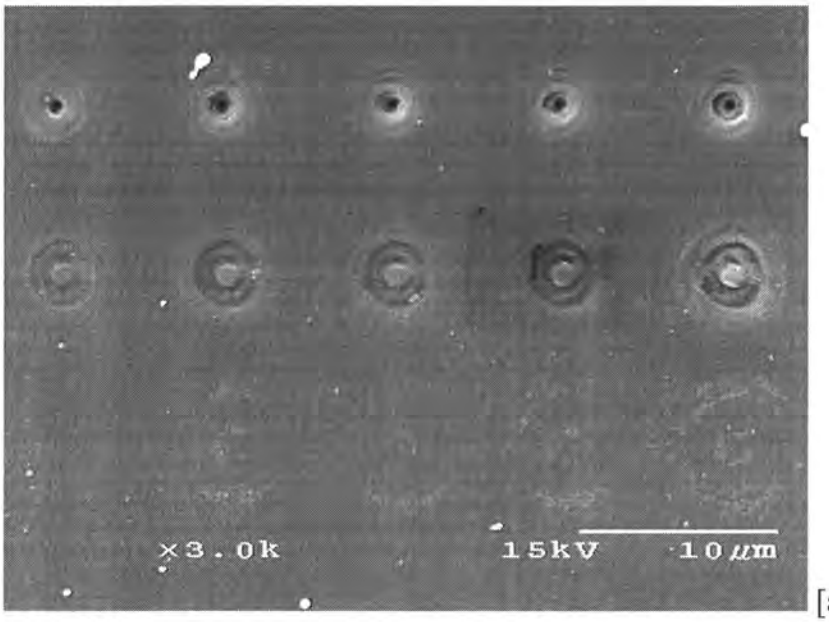

[a]

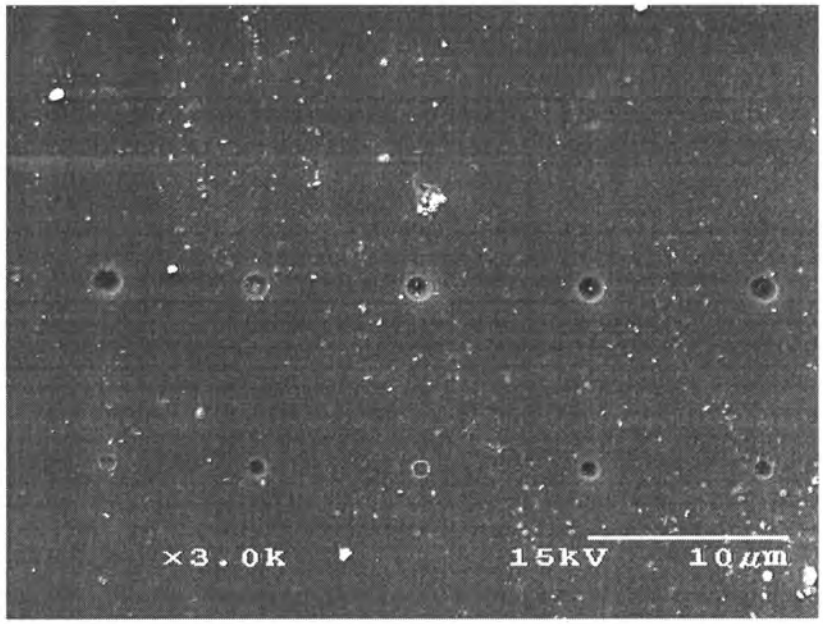

[b]

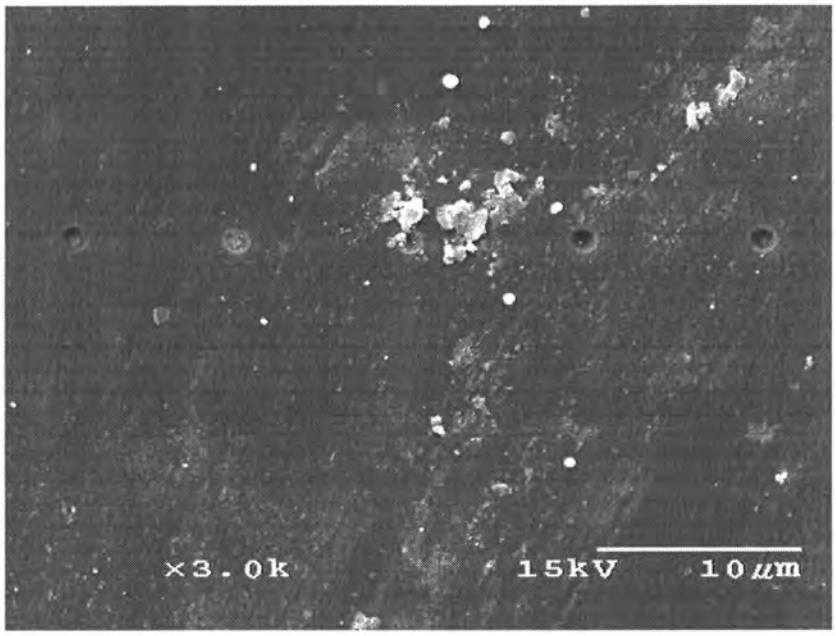

[c]

Figure 4.7 SEM micrographs of holes drilled a) 2000 nJ b) 630 nJ c) 200 nJ. Exposure time varies from 8-32 ms (from left to right).

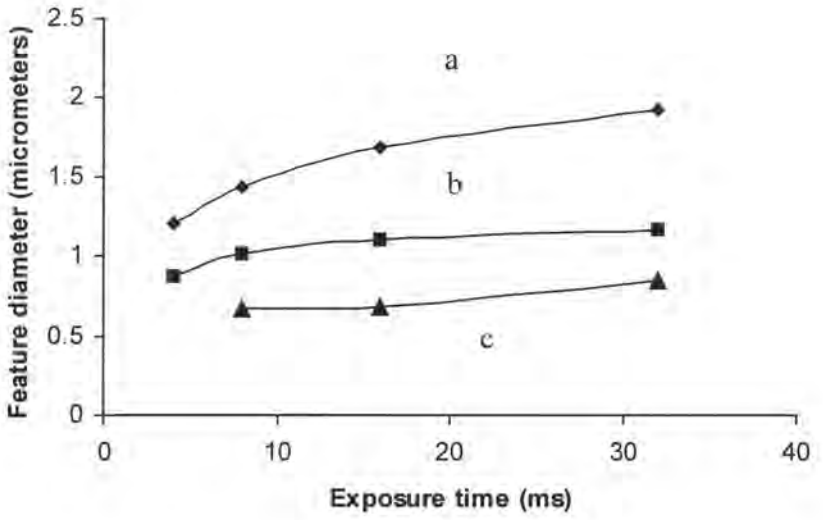

Figure 4.8. Variation of feature diameter (μm) against exposure time (s) for e = a) 2000 nJ b) 630 nJ c) 200 nJ.

AFM analysis was performed on a few holes to ascertain the hole geometry, recast layer formation and surface smoothness. Figure 4.9 shows the AFM images of holes produced with different pulse energies. For lower pulse energy, edge definition is excellent, clean hole interior and little debris or recast layer is observed around the hole. For higher pulse energies, the recast layer exists inside the hole.

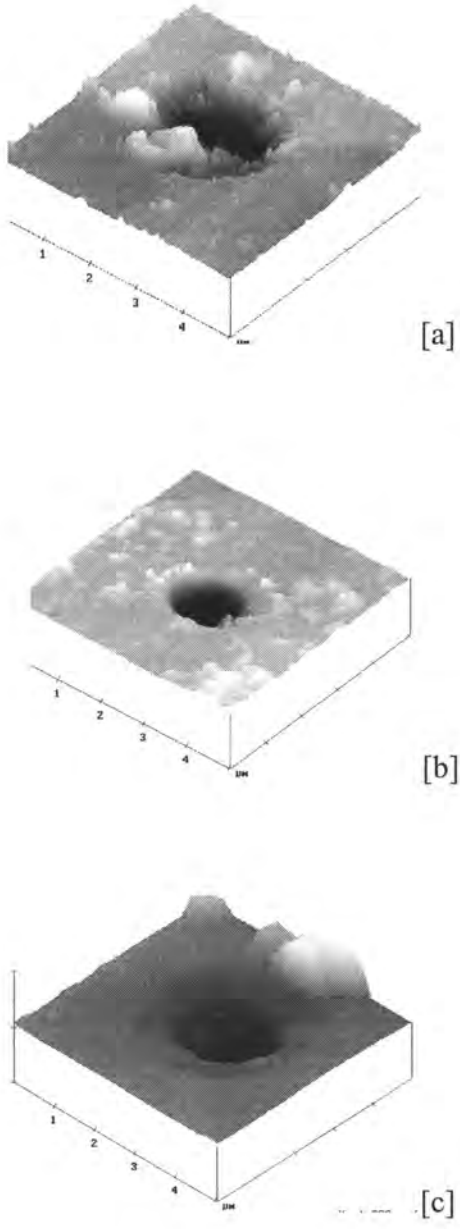

Figure 4.9. AFM pictures of holes in region D at E = a) 2000 nJ b) 630 nJ (32 ms) and c) 630 nJ (8ms). ***Exposure time in parentheses.***

Discussion

It is clear from this work that ultra-short pulsed Ti:Sapphire laser provided negligible collateral heating and shock-wave damage in single crystal diamond leading to unprecedented precision. By comparison, the long-pulsed Q-switched Nd:YAG and excimer lasers heat the diamond significantly and cause undesirable effects such as graphitization, large heat-affected-zone (HAZ), lower aspect ratio of holes, and inferior optical, electrical, and mechanical properties [5,9]. Being an optically transparent material, diamond requires the presence of defects such as micro-voids and impurities in order for the laser beam to create optical damage and enhance the light-absorption characteristics. The extreme intensity associated with femtosecond pulsed lasers offer marked improvements in light absorption by the material due to multiphoton absorption and avalanche ionization [6,10, 11]. In femtosecond pulse regime, the laser energy deposition into electrons occurs in less time than the transfer time to the lattice (<10 ps), creating a "hot electron" plasma and negligible heat transfer and shock wave damage to the lattice. Direct vaporization results in high precision. For nanosecond pulses, the energy transfer from the electrons to the ions is significant, and the heat diffusion involves much larger volume than the focus volume. Consequently, explosive ejection of liquid droplets occurs from the sample and forms recast layer as well as holes with uncontrolled dimensions. The femtosecond pulsed laser effects are attributed to enhanced energy coupling, reduced threshold energy fluence, precise spatial control of ablation with reduced collateral thermal damage, and absence of hydrodynamic motion of the ablated material during the pulse [10-14].

Damage Threshold

In ultra-short pulsed laser machining, it is important to work just above the damage threshold for producing clean ablation with potential for nanoscale features. Threshold is the energy fluence that produces damage with the following characteristics: ablation of a few atomic layers of material, melting or boiling of a small volume, and formation of structural defects and shallow cavity [10]. Since these features are often difficult to resolve, Stuart et al. [10] defines the damage threshold as any visible permanent modification to the surface with a feature size of 0.5 μm. Using this definition, the damage threshold for Type IIa diamond for 200-fs pulses was calculated using the experimental data.

The diameter D of an ablated region can be directly related to the energy fluence as [15]:

$$D^2 = 2 * w_o^2 \ln \frac{F_o}{F_{th}}$$

where, w_o= spot radius, F_o = Energy fluence = 2 E/π w_o^2 (Gaussian beam), E = pulse energy, and F_{th} = material-dependent threshold fluence. A plot of the square of damage diameter, D^2, against the logarithm of energy fluence (based on pulse energy range 200 nJ-2000 nJ, spot size of 3μm, number of pulses 2) was made to obtain the ablation threshold (the extrapolation of D to 0.5μm). The calculated value of F_{th} for 2 pulses is 3.5 J/cm^2.

Ablation threshold for multiple pulses, $F_{th}(N,\tau)$, can be related to the single-pulse threshold by a power-law expression given by [16]:

$$F_{th}(N,\tau) = F_{th}(1,\tau) * N^{S-1}$$

where, N is the number of pulses, τ is the pulse width, and S is the degree of incubation with an approximate value of 0.7 [16]. Thus, the damage threshold for single-pulse ablation is 4

J/cm^2. The damage thresholds for Type IIa are listed for different lasers listed in Table 4.5 [5]. The reduced threshold compared to the lower-wavelength lasers is attributed to the role played by multiphoton absorption.

Table 4.5. Damage threshold data for type IIa diamond [5]

Laser	Wavelength (nm)	Pulse width	Energy fluence (J/cm^2)
ArF	193	15 ns	3
KrF	248	15 ns	28
TEA-CO_2	10600	50 ns	> 93
Ti: Sapphire	775	200 fs	4

Ablation threshold can also be obtained from a fundamental physics equation given by [12]:

$$F_{th} = \frac{\rho \Omega T}{\alpha}$$

where, ρ is the density (kg m^{-3}), Ω is the specific heat of evaporation (J/kg K), T is evaporation temperature (K), and α is the absorption coefficient (m^{-1}). α is determined as 7 x 10^5 m^{-1} by substituting Table 4.1 data and F_{th} = 4 J/cm^2. α is much larger than the linear absorption coefficient listed in Table 4.1. Diamond has a large optical band-gap, around 5.2 eV, which prevents it from readily absorbing photons above 227 nm. Therefore, a laser must create optical damage in the material before it efficiently absorbs the laser energy. This damage includes the generation of color centers, defect structures, and phase changes. This

analysis shows that multiphoton absorption is significant in high-intensity laser interaction that increased α by more than two orders of magnitude.

Ablation Depth Per Pulse

A two-temperature model is presented below to predict the temperatures of the electrons and correlate them with the ablation depth per pulse. The model considered only the electrons because the ultra-short pulses are much shorter than the electron lattice equilibration times, 200 fs pulse versus approximately 2 ps to achieve electronic equilibration with the lattice. The model assumed that the electrons absorb all the laser energy and then transported it into the lattice by thermal conduction after the pulse is ceased. A one-dimensional model was deemed adequate because the laser spot is much larger than the absorption depth.

The differential equation that describes the heat flow is [17]:

$$C_e \frac{\partial T_e}{\partial t} = -\frac{\partial Q(z)}{\partial z} - \gamma(Te - Ti) + S \qquad \text{Electron}$$

$$C_i \frac{\partial T_i}{\partial t} = \gamma(T_e - T_i) \qquad \text{Lattice}$$

The left side of the equation is the time dependence of the temperature, and the right side governs the spatial variations. Ce and Ci are the electron and lattice heat capacity at constant volume, S is the laser heating source term, γ is the parameter governing the electron-lattice coupling, Q(z) is the heat flux and T_e and T_i are the electron and lattice temperatures respectively. Equation (3.4) was solved analytically in a femtosecond timescale to yield the electron temperature,

$$T_e(t) = \sqrt{\left(T_0 2 + \frac{2I_a\alpha}{C_e'} t \exp(-\alpha z) \right)}$$

Here I(t) = I_0 is assumed constant, $I_a = I_0 A$ where A = 1-R where R is the reflectivity and $T_0 = T_e(0)$ is the initial temperature.

At the end of the laser pulse, the electron temperature is given by

$$T_e(\tau_L) \cong \sqrt{\frac{2F_a\alpha}{C_e'}} \exp(-\frac{z}{\delta})$$

where, T_e (τ_L) >> T_0 is assumed, $F_a = I_a\tau_L$ is the absorbed laser fluence and $\delta = 2/\alpha$ is the skin depth. Here Ce' is a constant given by $C_e' = C_e/T_e$. An issue that must be resolved before using the above equation for calculating the electron temperatures is the specific heat of diamond. Since the thermal properties of diamond are dominated by phonon modes, the commonly tabulated heat capacities and thermal conductivity are unsuitable for this application, as they would be for a metal such as copper. Therefore, the heat capacity of the electrons had to be modeled using methods from solid-state physics [18]. A fairly accurate model is the free-electron model that uses Fermi-Dirac statistics. In this model only the electrons near the Fermi surface are able to conduct energy (The Fermi surface is defined as the highest occupied level when the material is at absolute zero). Metals have empty electronic states just above the filled states and this make the free-electron model highly accurate for modeling them. Diamond does not behave this way, as the next available electron states are over 5 eV above the highest filled states [19]. In order to deal with this, a theoretically calculated, density of states (DOS) was used to determine the electron distribution, and above the maximum energy of this distribution (around 14 eV), the electron states are assumed to be free-electron-like. The DOS is simply a function [p (ε)] that

indicates the number of available energy states for an electron available to occupy at any given energy. In diamond the valence electrons are located in a filled band that exists from – 21.0 eV to 0 eV, and the conduction band starts at 5.2 eV and continues up from there. Since we are predicting extremely high excitation states, the highest energy of the conduction band states needs to be considered in excess of 14 eV. The free-electron approximation was used for the states available higher than 14 eV and this was done by taking the equation for the free electron density of states [18] and subtracting 5.2 eV from the energy to compensate for the band gap. The number of states per volume present in diamond is the valence of the atom (carbon = 4), times the number of atoms per unit cell, (for diamond this is 8), divided by the volume of the unit cell. At absolute zero, only the states below 0 eV are filled. As the electrons are heated up, the states above the band gap become partially occupied. The Fermi function is used to describe the probability of occupation. The number of states in the material is always constant, regardless of temperature.

The equation that defines the number of occupied states :

$$n = \int_{-\infty}^{\infty} p(\varepsilon) \cdot f(\varepsilon)\, d\varepsilon$$

Here n is the number of occupied states, ε is the energy of a state, f(ε) is the Fermi function, and p(ε) is the function that describes the density of states. The Fermi function is:

$$f(\varepsilon) = \frac{1}{1 + e^{\left(\frac{\varepsilon - \mu}{k_b \cdot T}\right)}}$$

Its behavior is such that the function equals one when ε is significantly below the Fermi energy, and zero when ε is significantly above the Fermi energy. k_b is Boltzmann's

constant, which relates temperature to energy in the system. μ is the chemical potential of the system. Near the Fermi energy (within around k_bT) the function is some fraction less than one, and is indicative of the probability of occupancy. A material always has the same number of states "n" (unless electrons are lost in excitation, reducing their population), therefore "n" is used as a constant in these simulations. For diamond, "n" was a determined by calculating the number of valence electrons per volume. This was performed by taking the product of the number of valence electrons, four, and the number of atoms per unit cell, eight, and dividing by the volume of the unit cell, a cube 0.356 nm on a side.

The first step to calculate the heat capacity is to integrates (3.7) over all energy levels and solve for the chemical potential (μ) to keep n constant. This μ was then used to solve for the total energy of the electrons at a given temperature. Equation (3.8) shows the energy of the electrons u:

$$u = \int_{-\infty}^{\infty} \varepsilon \cdot p(\varepsilon) \cdot f(\varepsilon)\, d\varepsilon$$

This expression was then solved for the temperatures within the expected experimental range, and numerical differentiation was then used to generate a table of constant volume heat capacities (C_e). Figure 4.10 shows the heat capacity as a function of electron temperature. It was then used to predict the electron temperature distributions.

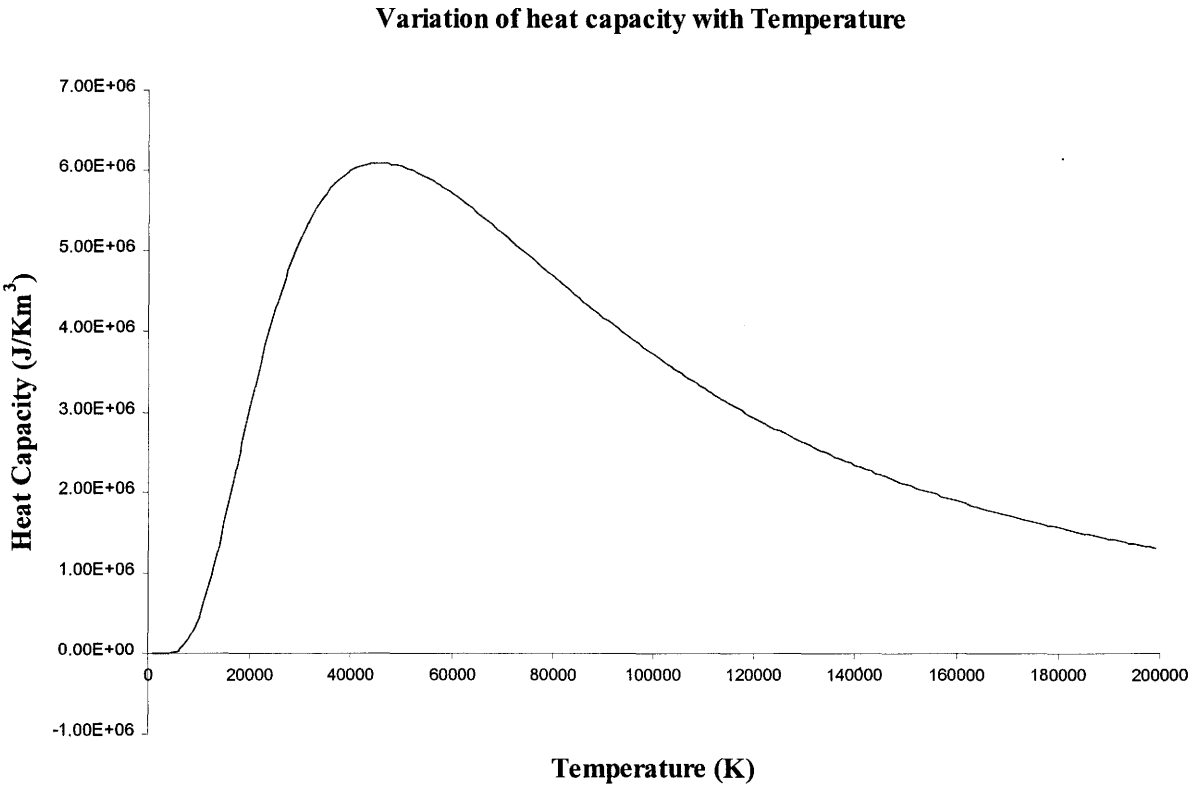

Figure 4.10.Variation of heat capacity C_e with electron temperature T_e

Estimation of electron temperature T_e for threshold fluence and experimental energies

Based on the curve of Figure 4.10, a relation was obtained between the heat capacity and the electron temperature. Equation 3.7 was then solved for the electron temperature at the threshold fluence of 4 J/cm^2 and at the various energies used in the experiments. Then value of z was varied from 1 nm to 10 μm to obtain different values of the electron temperatures. Figure 4.11 shows the variation of the electron temperatures with the depth z.

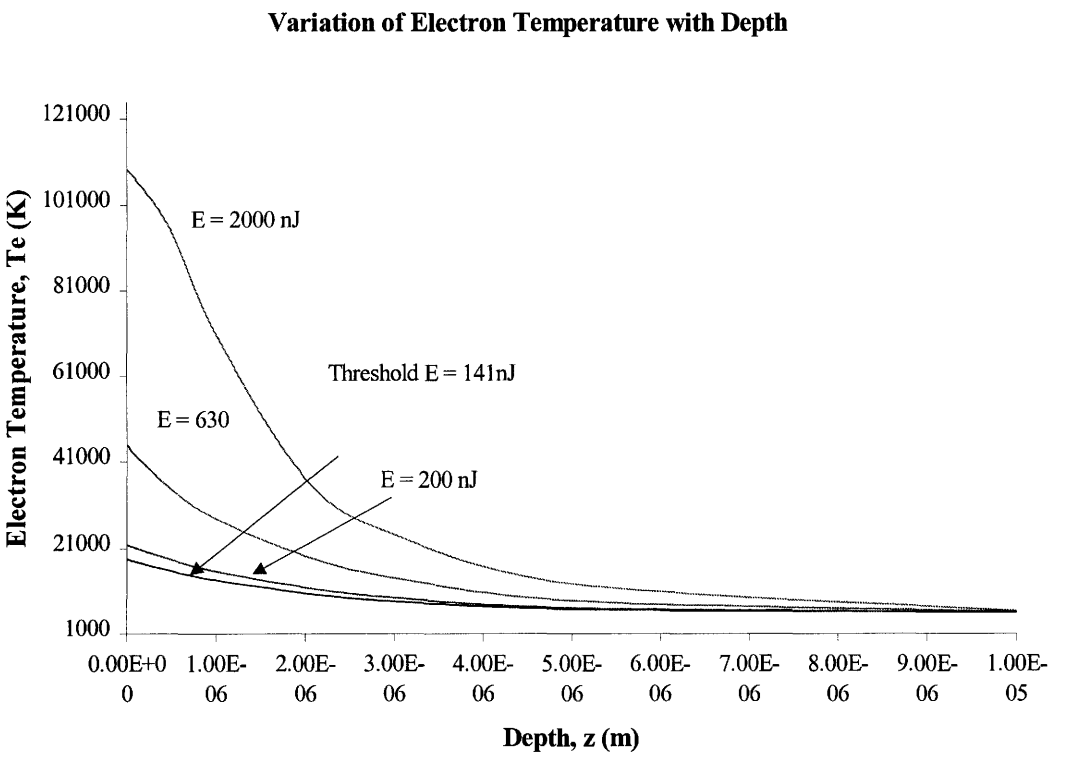

Figure 4.11. Variation of electron temperature with depth for threshold and experimental energies

From Figure 4.11, it is evident that electron temperatures fall with increasing depth. Also, at E = 200nJ, the curve closely follows the threshold energy curve. To predict the ablation depth per pulse we follow Stuart et al. definition of threshold fluence as mentioned earlier. Using Figure 4.11, we found the ablation depth per pulse for various energies, which is tabulated below.

Table 4.6. Ablation depth per pulse for different energies

Energy (nJ)	Ablation depth per pulse (μm)
2000	2
630	1.48
200	0.48

Conclusion

We have presented experimental results of femtosecond laser drilling and cutting of Type IIa diamond and compared it with a nanosecond pulsed laser. The results show that the femtosecond laser pulses cause ablation from the solid to the vapor phase with minimal recast layer and taper. The femtosecond pulsed laser has potential to drill deeper holes and narrow cuts even in high hardness materials like diamond. This feature combined with the cleanliness would be advantageous in applications requiring high precision.

Acknowledgements

The authors would like to thank Dr. Ali A. Said and Robert Maynard of Clark-MXR Inc. for processing the diamond sample using their femtosecond workstation, Dr. Warren Straszheim for help on obtaining SEM pictures. We would also like to thank Prof. Vladimir Tsukruk and Dr. Igor Luzinov for providing support for the AFM pictures. The authors would like to thank the financial support provided by the National Science Foundation (NSF) on the grant DMI – 9978633.

References

1. Prelas, M., G. Popovici, and L. Bigelow, eds. 1998. *Handbook of Industrial Diamonds and Diamond Films.* Marcel Dekker, Inc.
2. Bakon, A., and A. Szymanski. 1993. *Practical Uses of Diamond.* Ellis Horwood
3. Dyer, H.B. 1967. Physical and mechanical properties of diamond. *Proceedings of Industrial Diamond Conference* I to VIII.
4. Pierson, H.O. 1993. *Handbook of carbon, graphite, diamond and fullerenes.* Noyes Publications
5. Ralchenko, V.G., and S.M. Pimenov. 1998. Processing. *Handbook of Industrial Diamonds and Diamond Films.* Marcel Dekker Inc.
6. Shirk, M.D., and P.A. Molian. 1998. A review of ultrashort pulsed laser ablation of materials. *Journal of Laser Applications* 10 (2)
7. Strickland, D., and G. Mourou 1985. *Optical Communications.* 56: 219-224.
8. M. D. Shirk, P. A. Molian, and A. P. Malshe, J. Laser App. 10, 64-70 (1998).
9. R. Windholz and P. A. Molian J. Mater. Sci. 32, 4295-4301 (1997).
10. Stuart, B.C., M.D. Feit, S. Herman, A.M. Rubenchik, B.W. Shore, and M.D. Perry. 1996. Optical ablation by high-power short-pulse lasers. *Optical Society of America.* 13 (2) 459-468.
11. Liu, X., and G. Mourou. Laser Focus World. 1997: 101-118.
12. Momma, C., S. Nolte, B. Chichkov, F. Alvensleben, and A. Tunnermann. 1997. *Applied Surface Science.* 109:15-19.

13. Zhu, X., D.M. Villeneuve, A. Yu. Naumov, S. Nikumb, P.B. Corkum. 1999. Experimental study of drilling sub-10 μm holes in thin metal foils with femtosecond pulses. *Applied Surface Science* 152 (1999) 138-148.

14. Gudde, J., J. Hohlfeld, J.G. Muller, and E. Matthias, *Applied Surface Science*, 127-129, (1998)

15. Bonse, J. P. Rudolph, J. Kruger, S. Baudach and W. Kautek, *Applied Surface Science* 154-155 (2000) 659-663

16. Chichkov, B.N., C. Momma, S. Nolte, F. von Alvensleben, A. Tunnermann, Femtosecond, picosecond and nanosecond ablation of solids. *Appl. Phys. A* 63, 109-115 (1996).

17. Aschcroft, N. W. and N. D. Mermin, *Solid State Physics* (Harcourt Brace College Publishers NY, 1976),

18. Papaconstatopoulos, D.A. *Handbook of the Band Structure of Elemental Solids,* 230 (Plenum Press NY, 1986)].

CHAPTER 5. CONCLUSIONS / FUTURE WORK

Researchers have used different lasers for investigating the capabilities and laser-material interactions. These lasers include both continuous and pulsed lasers ranging in operating wavelengths from ultraviolet to far infrared regimes. For this work, Nd: YAG lasers with nanosecond pulses and Ti: sapphire lasers with femtosecond pulses were used. Experiments were conducted on different materials including Type IIa diamond, 316L steel and biomedical grade polymers. The phenomenon of nonlinearity was investigated coupled with both nanosecond and femtosecond pulses.

In the experiments conducted on nonlinear liquids, it was determined that certain liquids including carbon disulfide possess the capability of acting as liquid lenses. Ethylene glycol demonstrated the effect of filamentation of incident laser beam into multiple beamlets. A nonlinear wave equation was used to determine self-focusing depth for carbon disulfide. Experiments demonstrated that nonlinear liquids were able to reduce feature sizes by up to 100%. 316L stainless steel was the material used for the work. It was also determined that carbon disulfide required the least energy input in comparison to other liquids due to its high nonlinear refractive index.

The machining of Type IIa diamond was done using the Ti: sapphire femtosecond laser. The experiments were conducted to study the effects of the short pulses in terms of producing micron-sized structures. Different features were machined including blind holes, channels and through holes. Different modes of drilling (percussion and trepanning) were compared in terms of hole size and number of pulses. SEM analysis showed that hole sizes ranged from 0.65 – 100 μm and are free from taper. Damage threshold was determined to

be 4 J/cm^2 which, is considerably lower than other lasers and comparable to the shorter wavelength UV lasers.

Analytical models based on the two-temperature model were used to predict the electron temperatures. This data was used to calculate and graphically represent the ablation depth per pulse. The absence of taper and lower damage threshold proved the superior capability of femtosecond lasers in the micromachining of diamond. Raman spectroscopy revealed that the machined diamond surface was chemically pure.

Experiments conducted on Type IIa diamond using nanosecond pulsed Nd: YAG lasers demonstrated the deleterious effects of longer pulses. Holes drilled using the laser, showed large HAZ and thermal shocking around the feature.

Femtosecond pulses were used to machine biomedical grade latex. It was found that shorter pulses produced cleaner cuts devoid of HAZ and charring of the material. It was determined experimentally that use of shield gases helped to prevent undesirable heat effects on the material. A comparison study was done using Nd: YAG lasers and the results showed less than desirable characteristics of the machined region. SEM analysis was carried out to verify visual observations. A separate X-ray analysis of component elements revealed no major change in the plots in machined areas as compared to a virgin one.

Future work could include further study into the capability of nonlinear liquids to act as commercially viable lenses. Experiments carried out in this thesis were more concerned about the feasibility of the idea. However, to be commercially successful, machining of complex shapes in different dimensions has to be carried out. An important study would be to identify other liquids possessing high nonlinearity.

The interaction of femtosecond lasers with nonlinear liquids is an interesting area of research. The extremely high intensity associated with these lasers could possibly achieve greater self-focusing effects.

APPENDIX

EXPERIMENTAL INVESTIGATION

Introduction

Latex is one of the most widely used materials for many medical applications. The widespread use of latex stems from its many physical and chemical properties, which lend to it its suitability for the required applications. It is a complex intracellular product of a system of cells that synthesize a polymer (*cis*-1,4-polyisoprene), which is the main component of natural rubber. Latex contains hundreds of proteins, including enzymes that are involved in the biosynthesis of the rubber molecules. Protein fractions in latex are responsible for the allergic reactions that make latex allergy an important problem in anesthesia. By centrifugation a concentrated product is obtained. Latex is made heat-stable and elastic by vulcanization (heating in the presence of sulfur). Additional chemicals, such as accelerators, and antioxidants are added for strength, stretch and durability.

Properties of latex make it one of the most commonly used materials in the medical industry. It stretches without breaking, can be molded into shape and provides a barrier to water and germs. These include latex gloves, urinary catheters, tubing for barium enemas, rubber bungs in intravenous giving sets and sometimes drug vials, tourniquets used for taking blood, the rubber gum in self-adhesive bandages, dental drains and "rubber dams", some tapes, and anesthetic tubing. One of the most advanced applications of latex is in coronary angioplasty, a procedure for relieving blockades in the coronary arteries to restore normal blood flow.

Percutaneous transluminal coronary (PTCA)

PTCA is a procedure used to dilate (widen) narrowed arteries. A doctor inserts a catheter with a deflated balloon at its tip into the narrowed part of the artery. Then the balloon is inflated, compressing the plaque and enlarging the inner diameter of the blood vessel so blood can flow more easily. Then the balloon is deflated and the catheter removed. It's a less traumatic and less expensive alternative to bypass surgery for some patients with coronary artery disease.

In 10-20% of patients who've had PTCA, the dilated segment of the artery re-narrows within six months after the procedure. They may require either another PTCA or coronary artery bypass surgery. In this procedure the balloon used for inflation is usually made of latex, except in patients who are allergic to latex and the additives in latex. The main concern in angioplasty applications is the adhesion of the balloon to the catheter, which is used to deliver the balloon to the blocked artery for treatment. The catheters are usually made of silicone, polyurethane and some are metallic tipped.

The requirement of the medical firm was straight transverse cuts on the latex tubes. Razor cuts proved to be ineffective as the flexibility of latex caused tapering cuts, which were unacceptable. Laser cutting of the tubes was an alternative but with many conditions which needed to be met to comply with FDA (Food and Drug Administration) guidelines. The requirements were:

- Straight transverse cuts
- No HAZ
- No charring around the cut
- Chemical composition remains unchanged before and after the laser processing

The company used Nd: YAG lasers to perform the operation but the longer pulse widths associated with these lasers (nanoseconds) could not meet the requirements causing visible charring of the latex tubes. Ultrafast lasers were investigated as an alternative because of their extremely high intensities coupled with ultrashort (femtosecond) pulse widths, which gives them superior processing capability.

Materials and Methods

The material processed in the experiment was medical grade latex tube with nominal dimensions of 1.5mm O.D and a wall thickness of 200 microns. The tubes were mounted on a mandrel and the stepper motor for controlling the rotations was computer controlled. The motion of the stepper motor was set at one revolution every four seconds to enable a uniform diametric cut.

An oscillator-amplifier Ti: sapphire (femtosecond pulsed) laser system based on the chirped-pulsed-amplification (CPA) technique was used for cutting of latex tubes. The oscillator, having a small concentration (doping) of titanium dispersed uniformly in the sapphire, is capable of creating ultra-short pulses through mode locking by virtue of large bandwidth. However, the mode-locked oscillator produces low pulse energies that are not extendible to higher levels by *direct* amplification because the high intensity of the ultra-short pulsed beam tends to damage those materials that are used to amplify it. The method to avoid this damage is called chirped-pulse amplification (CPA) and involves stretching the pulse in time, then amplifying it, and finally compressing it to an ultra-short pulse. Stretching the pulse enables the intensity to be reduced and thereby prevents damage.

Table A.1. Laser specifications

Wavelength	Pulse Energy	Pulse Width	Repetition Rate
800 nm	400 μJ	120 fs	1 kHz

A 50-mm focusing lens was used to focus the output beam of the laser. The beam was defocused and the processing effects were studied. Ambient conditions were varied using shield gases including nitrogen and argon.

Results and Observations

Table A.2 shows the various processing parameters and conditions used for the experimental study. The tubes were positioned in different ways to study possible heat transfer from the mandrel. Figure A.1 illustrates the effect of ultrafast lasers under ambient conditions and under a shield gas Argon. It is clearly evident that use of a shield gas vastly improves on the cut quality, which was also confirmed visually. Figure A.2, is an SEM micrograph of effects of a nanosecond laser. The detrimental effects of a longer pulse were evident visually in terms of a visible charring zone around the cut. As reported earlier these defects are unacceptable under FDA guidelines for medical devices.

Table A.2. Processing Parameters and observations

Power (W)	Atmosphere	Focusing Setup	Time (s)	Sample Setup	Observation
0.2	Air	Focused	8	Supported	Visible HAZ
0.1	Argon	Focused	36	Supported	Clean
0.2			16		
0.4			8		
0.1	Argon	Focused	40	Unsupported	Clean
0.2			20		
0.4			8		
0.2	Argon	Defocused	24	Unsupported	Marginal charring
0.2	Air	Defocused	20	Unsupported	Marginal charring

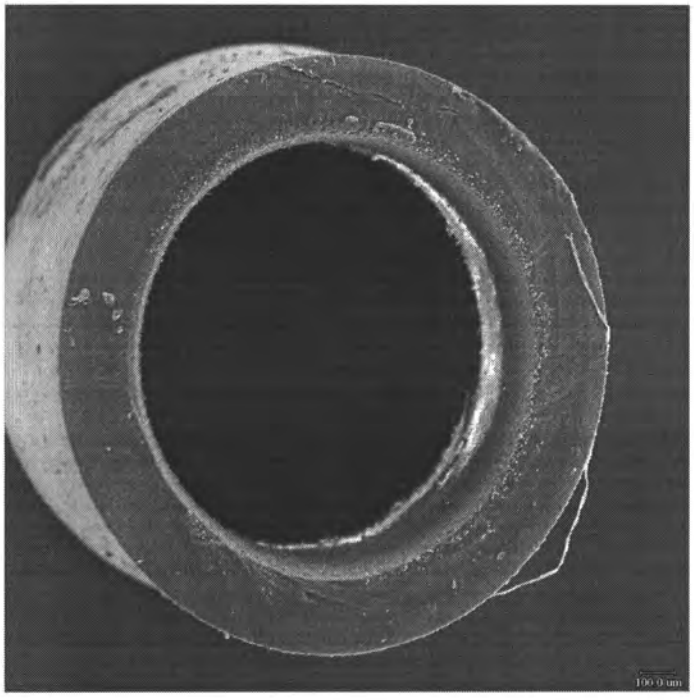

[a]

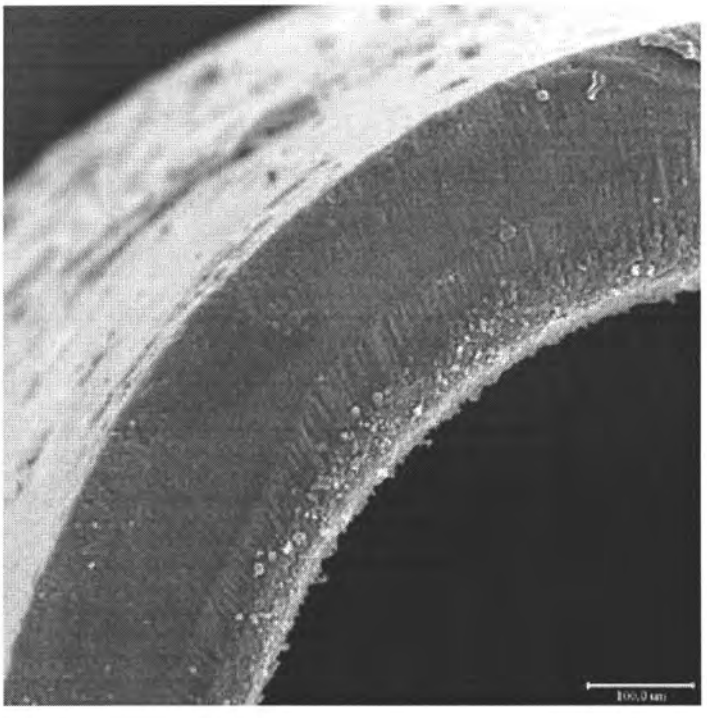

[b]

Figure A.1. SEM micrographs showing (a) femtosecond cutting in air and (b) cut surface under argon shield gas.

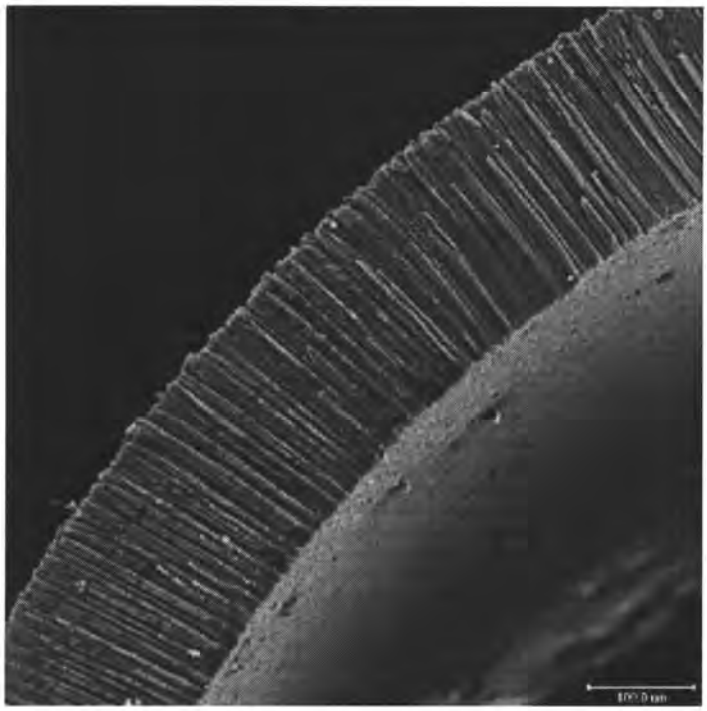

Figure A.2. SEM micrograph shows the cut surface of latex tube under Nd: YAG laser cutting.

Scanning electron pictures at higher magnification shown in Figure A.3, clearly reveal the deficiencies of a long pulsed laser in doing precision work. To determine the constituent elements, energy-dispersive x-ray spectroscopy (EDS) was performed on the cut surfaces. The femtosecond laser cut did not show any marked change in composition from the untreated surface.

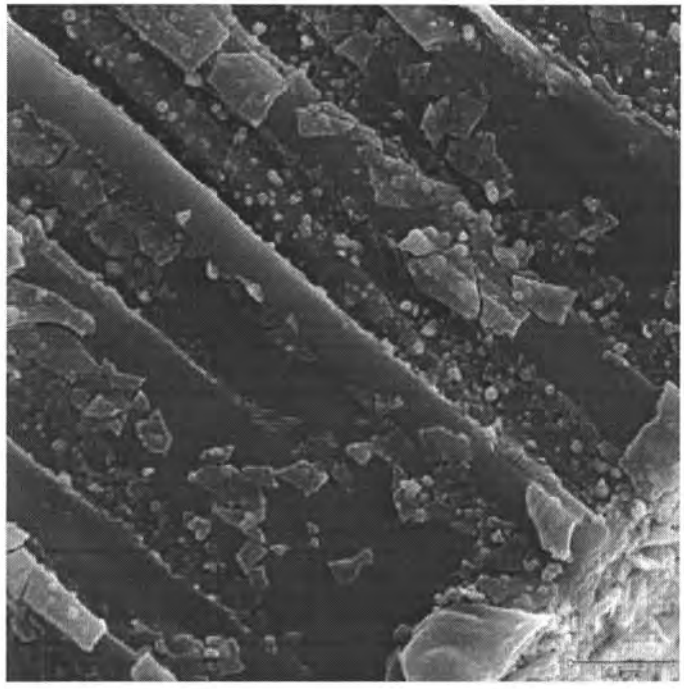

[a]

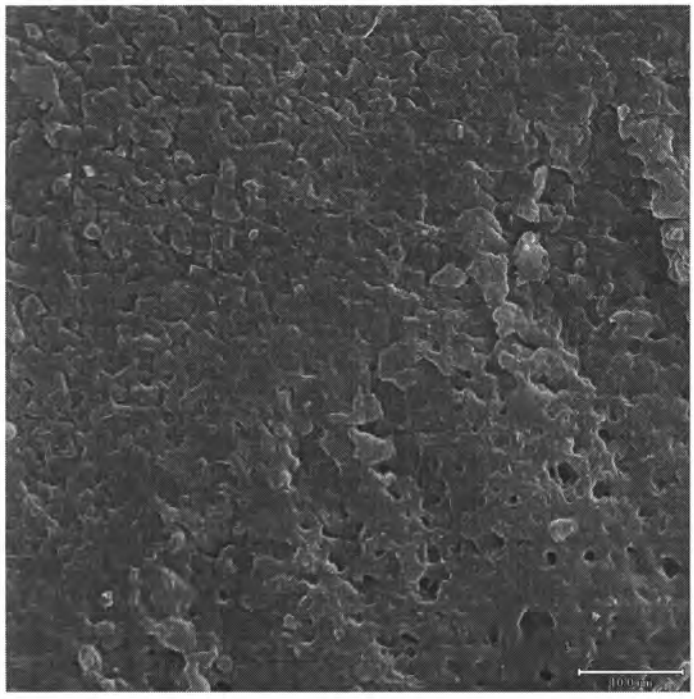

[b]

Figure A.3. SEM micrographs of cut surfaces at high magnification (1500X) for (a) Nd: YAG and (b) Ti: sapphire laser.

Discussion

The tests on the tubes revealed some interesting results. Ambient air proved to be deleterious to the tubes as they were subjected to significant charring. This was due to the presence of oxygen, which could have caused oxidation of latex. The high temperatures associated with laser cutting could have facilitated the oxidation leading to charring. The use of nitrogen as a shield gas did not cause significant improvement in the cut quality. However, argon proved to be a better shield gas. There was a dramatic improvement in the cut quality and no visual effect of charring was evident.

It was observed that supporting the sample over the mandrel increased the heat-affected zone. Heat transfer from the mandrel back to the inner dimensions of the tube could have caused it. This finding was confirmed by the presence of dark rings on the circumference of the mandrel due to the transmission of the laser beam on to the mandrel. A small overhang of the tube on the mandrel improved cut quality, as there was no transfer of heat from other sources. Defocusing the beam did not improve the quality of the cut but caused some marginal charring. This could be attributed to a larger beam size causing heat to be deposited around the cut.

Use of high input laser energy increased the cutting speed at the cost of quality. A low threshold fluence of latex could have caused excess energy to cause visible charring. Low energies were used to process the tubes but the cutting time was increased two-fold. However, it was of paramount importance to maintain the properties of the tube.

Conclusion

Based on the experiments and studies, the best processing characteristics were realized with a shield gas of argon and focusing the beam on the sample. Also, providing a small overhang for the tube over the mandrel improved the cut quality.

Acknowledgements

For the successful completion of this investigation, we would like to thank St. Jude Medical, MN for providing the materials. Also, we appreciate Dr. Straszheim for his assistance and inputs for completing the SEM analysis.